Decay widths of the spin-2 partners of the $X(3872)$

Miguel Albaladejo,[1,*] Feng-Kun Guo,[2,†] Carlos Hidalgo-Duque,[1,‡]
Juan Nieves,[1,§] and Manuel Pavón Valderrama[3,¶]

[1] *Instituto de Física Corpuscular (IFIC), Centro Mixto CSIC-Universidad de Valencia, Institutos de Investigación de Paterna, Aptd. 22085, E-46071 Valencia, Spain*

[2] *Helmholtz-Institut für Strahlen- und Kernphysik and Bethe Center for Theoretical Physics, Universität Bonn, D-53115 Bonn, Germany*

[3] *Institut de Physique Nucléaire, Université Paris-Sud, IN2P3/CNRS, F-91406 Orsay Cedex, France*

We consider the $X(3872)$ resonance as a $J^{PC} = 1^{++}$ $D\bar{D}^*$ hadronic molecule. According to heavy quark spin symmetry, there will exist a partner with quantum numbers 2^{++}, X_2, which would be a $D^*\bar{D}^*$ loosely bound state. The X_2 is expected to decay dominantly into $D\bar{D}$, $D\bar{D}^*$ and $\bar{D}D^*$ in d-wave. In this work, we calculate the decay widths of the X_2 resonance into the above channels, as well as those of its bottom partner, X_{b2}, the mass of which comes from assuming heavy flavor symmetry for the contact terms. We find partial widths of the X_2 and X_{b2} of the order of a few MeV. Finally, we also study the radiative $X_2 \to D\bar{D}^*\gamma$ and $X_{b2} \to \bar{B}B^*\gamma$ decays. These decay modes are more sensitive to the long-distance structure of the resonances and to the $D\bar{D}^*$ or $B\bar{B}^*$ final state interaction.

* Miguel.Albaladejo@ific.uv.es
† fkguo@hiskp.uni-bonn.de
‡ carloshd@ific.uv.es
§ jmnieves@ific.uv.es
¶ pavonvalderrama@ipno.in2p3.fr

I. INTRODUCTION

In the infinite quark mass limit, heavy quark spin-flavor symmetry (HQSFS) implies that the dynamics involving heavy quarks are independent of their spin or flavor. In this way, charm and bottom spectra can be related, up to corrections suppressed by $1/m_Q$ with m_Q the heavy quark mass. It should also be possible, in a given heavy flavor sector, to relate states with different spins. These relations are very useful in the study of composites that mix heavy and light quarks. In this work, we focus on hadronic molecular states composed by a heavy-light meson and a heavy-light antimeson ($P^{(*)}\bar{P}^{(*)}$, $P = D, \bar{B}$). These molecular states were predicted in the mid 70s [1, 2]. So far, the best experimental candidate to fit this molecular description is the $X(3872)$ resonance, first observed by the Belle Collaboration in 2003 [3], that can be thought as a $D\bar{D}^*$ bound state with $J^{PC} = 1^{++}$ (quantum numbers confirmed later on in Ref. [4]). Since then, many other new XYZ states which are good candidates to be *exotic* hadrons have been experimentally observed [5, 6].

Within the molecular description of the $X(3872)$, the existence of a X_2 [$J^{PC} = 2^{++}$] s-wave $D^*\bar{D}^*$ bound state was predicted in the effective field theory (EFT) approach of Refs. [7, 8]. As a result of the heavy quark spin symmetry (HQSS), the binding energy of the X_2 resonance was found to be similar to that of the $X(3872)$, *i.e.*,

$$M_{X_2} - M_{X(3872)} \approx M_{D^*} - M_D \approx 140 \text{ MeV}. \tag{1}$$

The existence of such a state was also suggested in Refs. [9–14]. Both the $X(3872)$ and the X_2, to be denoted by $X_2(4013)$ in what follows, have partners in the bottom sector [15],[1] which we will call X_b and X_{b2}, respectively, with masses approximately related by

$$M_{X_{b2}} - M_{X_b} \approx M_{B^*} - M_B \approx 46 \text{ MeV}. \tag{2}$$

It is worthwhile to mention that states with 2^{++} quantum numbers exist as well as spin partners of the 1^{++} states in the spectra of the conventional heavy quarkonia and tetraquarks. However, the mass splittings would only accidentally be the same as the fine splitting between the vector and pseudoscalar charmed mesons, see Eq. (1).[2] For instance, the mass splitting between the first radially excited charmonia with 2^{++} and 1^{++} in the well-known Godfrey–Isgur quark model is 30 MeV [17], which is much smaller than the value in Eq. (1). In a quark model calculation with screened potential, the $2^{++} - 1^{++}$ mass splitting for the $2P$ charmonia is around 40 MeV [18]. As

[1] In Ref. [15], the bottom and charm sectors are connected by assuming the bare couplings in the interaction Lagrangian, see Eq. (A6), to be independent of the heavy quark mass. This assumption will also be used throughout this work.

[2] Were these states due to threshold cusps, the splittings would be the same as those of the hadronic molecules. However, it was shown in Ref. [16] that narrow near threshold peaks in the elastic channel cannot be produced by threshold cusps.

for the tetraquark states, the corresponding mass splitting predicted in Ref. [19] is 70 MeV, which is again much smaller than $M_{D^*} - M_D$. Notice that it is generally believed that the $\chi_{c2}(2P)$ has been discovered [20, 21], and its mass is much lower than $2M_{D^*}$. Therefore, we conclude that a possible discovery of a 2^{++} charmonium-like state with a mass around 4013 MeV as a consequence of HQSS [22] would provide a strong support for the interpretation that the $X(3872)$ is dominantly a $D\bar{D}^*$ hadronic molecule. It is thus very important to search for such a tensor resonance, as well as the bottom analogues, in various experiments and in lattice QCD (LQCD) simulations.

Some exotic hidden charm sectors on the lattice have been recently studied [23–27], and evidence for the $X(3872)$ from $D\bar{D}^*$ scattering on the lattice has been found [24], while the quark mass dependence of the $X(3872)$ binding energy was discussed in Refs. [28, 29]. The 2^{++} sector has not been exhaustively addressed yet in LQCD, though a state with these quantum numbers and a mass of $(m_{\eta_c} + 1041 \pm 12)$ MeV$= (4025 \pm 12)$ MeV, close to the value predicted in Refs. [7, 8], was reported in Ref. [23]. The simulation used dynamical fermions, novel computational techniques and the variational method with a large basis of operators. The calculations were performed on two lattice volumes with pion mass $\simeq 400$ MeV. There exists also a feasibility study [30] of future LQCD simulations, where the EFT approach of Refs. [7, 8] was formulated in a finite box.

On the other hand, despite the theoretical predictions on their existence, none of these hypothetical particles has been observed so far. Nevertheless, they are being and will be searched for in current and future experiments such as BESIII, LHCb, CMS, Belle-II and PANDA. It is thus of paramount importance to provide theoretical estimates on their production rates in various experiments, as well as the dominant decay modes and widths.[3] The production of these states in hadron colliders and electron–positron collisions has been studied in Refs. [31, 32]. In this work, we will investigate the dominant decay modes of the spin-2 partners of the $X(3872)$, i.e. the $X_2(4013)$ and X_{b2}, and provide an estimate of their decay widths.

Besides, we will also discuss the radiative $X_2 \to D\bar{D}^*\gamma$ and $X_{b2} \to \bar{B}B^*\gamma$ transitions. These decay modes are more sensitive to the long-distance structure of the resonances and might provide valuable details on their wave-functions. The situation is similar to that of the $X(3872) \to D^0\bar{D}^0\pi^0$ decay studied in Refs. [33, 34]. Also here, the widths will be affected by the $D\bar{D}^*$ or $B\bar{B}^*$ final state interaction (FSI). FSI effects are expected to be large because they should be enhanced by the presence of the isovector $Z_c(3900)$ and $Z_b(10610)$ resonances located near the $D\bar{D}^*$ and $\bar{B}B^*$ thresholds, respectively. Besides, FSI corrections will be also sensitive to the negative C-parity isoscalar $D\bar{D}^*$ or $\bar{B}B^*$ interaction. Eventually, precise measurements of these radiative

[3] If a resonance is too broad, say $\Gamma \gtrsim 200$ MeV, it would be very difficult to be identified since it is highly nontrivial to distinguish the signal for a broad resonance from various backgrounds.

decay widths might provide valuable information on the interaction strength in this sector, which would be important in understanding the $P^{(*)}\bar{P}^{(*)}$ system and other exotic systems related to it through heavy quark symmetries [15, 35].

The structure of the paper is as follows. First in Sect. II, we briefly discuss the relation of the charm and bottom 2^{++} states with the $X(3872)$ resonance, and in Sect. III we present our predictions for the $X_2 \to D\bar{D}, D\bar{D}^*$ hadron decays and the $X_{b2} \to B\bar{B}, B\bar{B}^*$ ones in the bottom sector. In Sect. IV, the X_2 and X_{b2} radiative decays are investigated, paying special attention to the loop mechanisms responsible for the FSI contributions. The conclusions of this work are outlined in Sect. V and in addition, there are three Appendices. In the first one (Appendix A), we collect different heavy meson Lagrangians used through this work, while the validity of the perturbative treatment of the $D\bar{D}$ for the X_2 is discussed in the second one (Appendix B). Finally, in Appendix C, we give some details on the evaluation of different three-point loop functions that appear in the computation of the hadronic and radiative decays.

II. HQSFS, THE $X(3872)$ RESONANCE AND THE CHARM AND BOTTOM X_2 STATES

A. $X(3872)$

As mentioned, we start assuming the $X(3872)$ to be a positive C-parity $D\bar{D}^*$ bound state, with quantum numbers $J^{PC} = 1^{++}$. At very low energies, the leading order (LO) interaction between pseudoscalar and vector charmed $(D^0, D^+, D^{*0}, D^{*+})$ and anti-charmed $(\bar{D}^0, D^-, \bar{D}^{*0}, D^{*-})$ mesons can be described just in terms of a contact-range potential, which is constrained by HQSS [7, 8, 15]. Pion exchange and particle coupled-channel[4] effects turn out to be sub-leading [7, 36]. For the case of the $X(3872)$, isospin breaking is important [37] as this bound state is especially shallow. The energy gap between the $D^0\bar{D}^{*0}$ and D^+D^{*-} channels is around 8 MeV, which is much larger than the $X(3872)$ binding energy with respect to the $D^0\bar{D}^{*0}$ threshold. As a consequence, the neutral $(D^0\bar{D}^{*0})$ and charged (D^+D^{*-}) channels should be treated independently. The coupled-channel[5] contact potential in the 1^{++} sector is given by [8] (see also Appendix A 1)

$$V_{X(3872)} = \frac{1}{2}\begin{pmatrix} C_{0X}+C_{1X} & C_{0X}-C_{1X} \\ C_{0X}-C_{1X} & C_{0X}+C_{1X} \end{pmatrix}, \tag{3}$$

with C_{0X} and C_{1X} low energy constants (LECs) that need to be fixed from some input. This interaction is used as kernel of the Lippmann–Schwinger equation (LSE) in the coupled channel

[4] We do not refer to charge channels, but rather to the mixing among the $D\bar{D}$, $D\bar{D}^*$, $D^*\bar{D}^*$ pairs in a given IJC (isospin, spin and charge conjugation) sector.

[5] Actually, positive C-parity combinations in both the neutral $D^0\bar{D}^{*0}$ and charged $D^+\bar{D}^{*-}$ channels are being considered.

space in the 1^{++} sector,

$$T(E;\vec{p}\,',\vec{p}) = V(\vec{p}\,',\vec{p}) + \int \frac{d^3\vec{q}}{(2\pi)^3} V(\vec{p}\,',\vec{q}) \frac{1}{E - \vec{q}^{\,2}/2\mu_{12} - M_1 - M_2 + i\varepsilon} T(E;\vec{q},\vec{p}) \ , \tag{4}$$

with M_1 and M_2 the masses of the involved mesons, $\mu_{12}^{-1} = M_1^{-1} + M_2^{-1}$, E the center of mass (c.m.) energy of the system and $\vec{p}$ ($\vec{p}\,'$) the initial (final) relative three momentum of the $D\bar{D}^*$ pair in the c.m. frame. The used normalization is such that above threshold $[E > (M_1 + M_2)]$, the single channel elastic unitary condition is $\mathrm{Im}\, T^{-1}(E) = \mu_{12} k/(2\pi)$ with $k = \sqrt{2\mu_{12}\,(E - M_1 - M_2)}$. The discussion is similar for any other J^{PC} sector. Due to the use of contact interactions, the LSE shows an ill-defined ultraviolet (UV) behavior, and requires a regularization and renormalization procedure. We employ a standard Gaussian regulator (see, *e.g.* [38])

$$\langle \vec{p}\,|V|\vec{p}\,'\rangle = C_{IX}\ e^{-\vec{p}^{\,2}/\Lambda^2}\ e^{-\vec{p}\,'^2/\Lambda^2}, \tag{5}$$

with C_{IX} any of the LECs of Eq. (3) in the case of the $X(3872)$, or the relevant ones for any other J^{PC} sector. We take cutoff values $\Lambda = 0.5 - 1$ GeV [7, 8], where the range is chosen such that Λ will be bigger than the wave number of the states, but at the same time it will be small enough to preserve HQSS and prevent that the theory might become sensitive to the specific details of short-distance dynamics.[6] The dependence of the results on the cutoff, when it varies within this window, provides a rough estimate of the expected size of sub-leading corrections. Bound states correspond to poles of the T-matrix below threshold on the real axis in the first Riemann sheet (RS) of the complex energy, while the residues at the pole give the s-wave couplings of the state to each channel ($D^0\bar{D}^{*0}$ and D^+D^{*-} in the case of the $X(3872)$ resonance[7]).

The LECs C_{0X} and C_{1X} can in principle be determined [8] from $M_{X(3872)} = (3871.69 \pm 0.17)$ MeV (mass average quoted by the PDG [5]) and the isospin violating ratio of the decay amplitudes for the $X(3872) \to J/\psi\pi\pi$ and $X(3872) \to J/\psi\pi\pi\pi$, $R_{X(3872)} = 0.26 \pm 0.07$ [39]. The ratio is given by (see Eq. (80) of Ref. [8])

$$R_{X(3872)} = \frac{\hat{\Psi}_{\rm n} - \hat{\Psi}_{\rm c}}{\hat{\Psi}_{\rm n} + \hat{\Psi}_{\rm c}} \tag{6}$$

where $\hat{\Psi}_{\rm n,c}$ give the average of the neutral and charged wave function components in the vicinity of the origin, and are related to the LECs introduced in Eq. (3) by [37]

$$\frac{\hat{\Psi}_{\rm n}}{\hat{\Psi}_{\rm c}} = \frac{1 - G_2\,(C_{0X} + C_{1X})/2}{G_2\,(C_{0X} - C_{1X})/2} = \frac{G_1\,(C_{0X} - C_{1X})/2}{1 - G_1\,(C_{0X} + C_{1X})/2} \tag{7}$$

[6] However, as will be shown later on, the situation is more complicated in the two-body d-wave hadronic decays.

[7] For instance, in the case of the $X(3872)$, we have

$$\left(g_0^X\right)^2 = \lim_{E \to M_X(3872)} [E - M_X(3872)] \times T_{11}(E) \ ,$$
$$g_0^X g_c^X = \lim_{E \to M_X(3872)} [E - M_X(3872)] \times T_{12}(E) \ ,$$

where T_{ij} are the matrix elements of the T-matrix solution of the UV regularized LSE.

where the neutral and charged loop functions, $G_1 = G_{D^0\bar{D}^{*0}} = G_{D^{*0}\bar{D}^0}, G_2 = G_{D^+D^{*-}} = G_{D^{*+}D^-}$, are defined in Eq. (A12), and should be evaluated at the $X(3872)$ pole mass. We use $m_{D^0} = (1864.84 \pm 0.07)$ MeV, $m_{D^+} = (1869.61 \pm 0.10)$ MeV, $m_{D^{*0}} = (2006.96 \pm 0.10)$ MeV and $m_{D^{*+}} = (2010.26 \pm 0.07)$ MeV [5]. Note that $m_{D^0} + m_{D^{*0}} = (3871.80 \pm 0.12)$ MeV, and the uncertainty in the value of this lowest threshold affects the precision of the $X(3872)$ binding energy. We have taken into account this effect by adding in quadratures the PDG error of the $X(3872)$ mass and that of the neutral channel threshold and assign this new error to the mass of the resonance, that now reads $M_{X(3872)} = (3871.69 \pm 0.21)$ MeV. For the LECs, we obtain:

$$C_{0X} = -1.70^{+0.03}_{-0.07}\ (-0.731^{+0.006}_{-0.015})\,\text{fm}^2, \qquad C_{1X} = -0.09^{+0.54}_{-0.41}\ (-0.38^{+0.12}_{-0.10})\,\text{fm}^2\ , \tag{8}$$

for $\Lambda = 0.5(1.0)$ GeV. Errors, at the 68% confidence level (CL), have been obtained from a Monte Carlo (MC) simulation assuming uncorrelated Gaussian distributions for the two inputs $(M_{X(3872)}, R_{X(3872)})$. In the simulation, we have rejected MC samples for which the $X(3872)$ turned out to be unbound, since the scheme of Ref. [8] only allows to determine the properties of the resonance when it is bound.

B. $X_2(4013)$: $J^{PC} = 2^{++}$, charm sector

HQSS predicts that the s-wave $D^*\bar{D}^*$ interaction in the 2^{++} sector is, up to corrections suppressed by the charm quark mass, identical to that in the $X(3872)$ sector (1^{++}) and given by Eq. (3) [7, 8]. Thus, in the 2^{++} sector, the potential in the $(D^{*0}\bar{D}^{*0})$, $(D^{*+}D^{*-})$ coupled channel space reads (see also Appendix A 1)

$$V_{2^{++}} = \frac{1}{2}\begin{pmatrix} C_{0X}+C_{1X} & C_{0X}-C_{1X} \\ C_{0X}-C_{1X} & C_{0X}+C_{1X} \end{pmatrix} + \mathcal{O}(q/m_c), \tag{9}$$

with the same structure and involving the same LECs that in the $X(3872)$ channel. Besides, in the above equation $m_c \sim 1.5$ GeV is the charm quark mass and $q \sim \Lambda_{\rm QCD}$, a scale related to the light degrees of freedom. Taking $\Lambda_{\rm QCD} \sim 300$ MeV [5], corrections of the order of 20% to the interaction predicted by HQSS cannot be discarded[8]. Nevertheless, it seems natural to expect a 2^{++} $D^*\bar{D}^*$ loosely bound state (X_2), the HQSS partner of the $X(3872)$, and located in the vicinity of the $D^{*0}\bar{D}^{*0}$ threshold ($\sim$ 4014 MeV) [7, 8, 15]. This is illustrated in the X_2 binding energy distributions depicted in Fig. 1. Neglecting the $\mathcal{O}(q/m_c)$ corrections to the LECs, and using those

[8] The two type of uncertainties (HQSS subleading corrections and errors inherited from the inputs) affecting the determination of the LECs in the 2^{++} sector are statistically uncorrelated, and should be accordingly added up. To that end, we use MC techniques as explained in the caption of Fig. 1.

obtained from the $X(3872)$ resonance, we find a clear signal (blue histograms) of a weakly bound state. However, the case is less robust when the latter corrections are taken into account. Thus, because of the additional 20% HQSS uncertainty, the area below the red shaded $\Lambda = 0.5$ GeV ($\Lambda = 1$ GeV) histogram is only 0.77 (0.68). This means that approximately a 23% (32%) of $X(3872)$ events $[(M_{X(3872)}, R_{X(3872)})$ MC samples] do not produce a X_2 pole in the first RS, since the strength of the resulting interaction in the 2^{++} sector would not be attractive enough to bind the state, though a virtual state in the second RS will be generated instead. Given the existence of the $X(3872)$ as a $D\bar{D}^*$ molecule, if the X_2 resonance exists, we would expect its mass (binding energy) to lie most likely in the interval $[2m_{D^{*0}}, 4006$ MeV] ($[0, 8]$ MeV), as shown in Fig. 1. Note that the discussion in Ref. [15] was simpler, because there we worked in the isospin symmetric limit and used the averaged masses of the heavy mesons, which are larger than those of the physical D^0 and D^{*0} mesons.

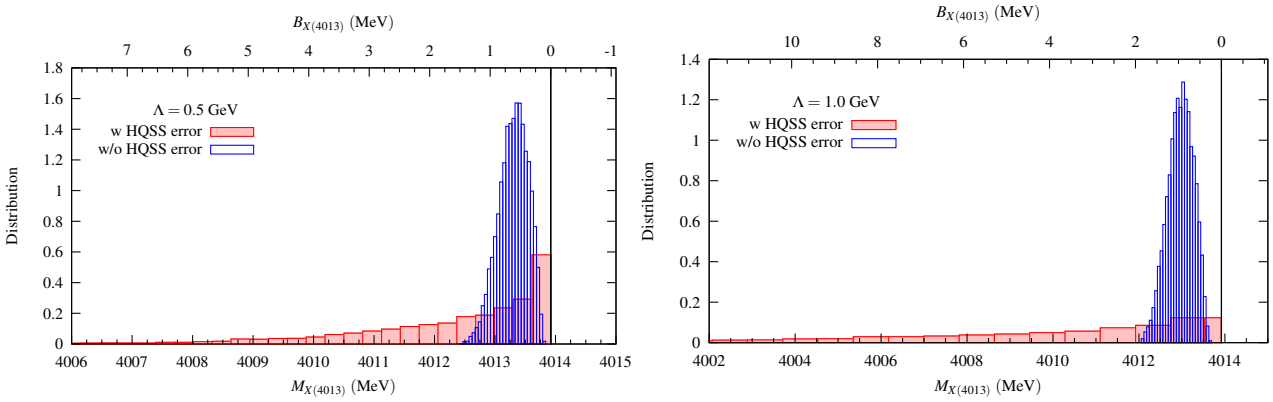

FIG. 1. X_2 binding energy histograms obtained from the interaction of Eq. (9) using LECs distributions determined from the $X(3872)$ resonance inputs (blue) or using LECs distributions additionally modified to account for the HQSS systematic error (red). Left and right plots correspond to UV cutoffs of 0.5 and 1 GeV, respectively. MC sample $(C_{0X} + C_{1X}, C_{0X} - C_{1X})$ pairs fitted to the input $(M_{X(3872)}, R_{X(3872)})$ distributions are first generated and are used to evaluate the X_2 mass. $X(3872)$ mass trials above threshold are rejected. To evaluate the red shaded histogram, and to account for the HQSS 20% uncertainty in the 2^{++} interaction, each of the members of any MC sample $(C_{0X} + C_{1X}, C_{0X} - C_{1X})$ pair is multiplied by independent $\mathrm{N}(\mu = 1, \sigma = 0.2)$ Gaussian distributed random quantities $r_\pm$.

For later use, we also need the couplings of the X_2 to its neutral $(D^{*0}\bar{D}^{*0})$ and charged $(D^{*+}D^{*-})$ components, $g_0^{X_2}$ and $g_c^{X_2}$, respectively. They turn out to be slightly different because the X_2 resonance is an admixture of isospin 0 and 1, since its binding energy is much smaller than the

energy difference between the two thresholds [8, 37]. Considering the HQSS uncertainties, we find:

$$10^2 g_0^{X_2} = 1.4^{+1.1}_{-0.4} \ \ (1.5^{+1.1}_{-0.4}) \ \ \text{MeV}^{-1/2} \ , \tag{10}$$

$$10^2 g_c^{X_2} = 1.5^{+1.4}_{-0.2} \ \ (1.3^{+1.3}_{-0.3}) \ \ \text{MeV}^{-1/2} \ , \tag{11}$$

for $\Lambda = 0.5(1.0)$ GeV.

C. X_{b2}: $J^{PC} = 2^{++}$, bottom sector

Owing to the heavy flavor symmetry, the LO 2^{++} $B^*\bar{B}^*$ interaction is given by Eq. (9) as well, and thus we should also expect a 2^{++} $B^*\bar{B}^*$ bound state (X_{b2}), the HQSFS partner of the $X(3872)$, located close to the $B^*\bar{B}^*$ threshold (~ 10650 MeV) [15]. The X_{b2} binding energy distributions are shown in Fig. 2 for the two UV cutoffs employed in this work. We have used the same masses for the neutral and charged mesons, $m_B = (m_{B^0} + m_{B^+})/2 = 5279.42$ MeV and $m_{B^*} = 5325.2$ MeV. Note that, according to the PDG [5], $|(m_{B^{*0}} - m_{B^0}) - (m_{B^{*+}} - m_{B^+})| < 6$ MeV CL=95.0%, and $m_{B^0} - m_{B^+} = (0.32 \pm 0.06)$ MeV, from where we might expect isospin breaking effects for the B^* mesons to be significantly smaller than in the charm sector. In Ref. [15] we found that the binding energy of the X_{b2} state is significantly larger than that of its counterpart in the charm sector (X_2), around a few tens of MeV. Thus we do not expect any significant isospin breaking effects and the X_{b2} resonance would be a pure isoscalar ($I = 0$) state.

As can be seen in Fig. 2, in this case we have a robust prediction even when HQSS uncertainties (20%) are taken into account. We obtain the mass and the coupling from the residue at the pole for $\Lambda = 0.5$ (1.0) GeV:[9]

$$E_{X_{b2}} = 10631^{+7}_{-8} \left(10594^{+22}_{-26}\right) \text{MeV}, \qquad 10^2 g^{X_{b2}} = 5.9^{+2.9}_{-1.9} \left(6.4^{+2.8}_{-2.0}\right) \text{MeV}^{-1/2}. \tag{12}$$

This bound state, being isoscalar, equally couples to the neutral and charged components and, therefore: $g_0^{X_{b2}} = g_c^{X_{b2}} = \frac{1}{\sqrt{2}} g^{X_{b2}}$. Our predictions in Eq. (12), both for the mass and the $B^*\bar{B}^*$ coupling of the resonance show some dependence on the UV cutoff, which is to some extent diminished when HQSS uncertainties are taken into account. Nevertheless, this Λ dependence might hint to non-negligible sub-leading corrections (among others, pion exchange and coupled channel effects [7], which can be larger here than in the charm sector due to the larger binding energy and larger meson masses). We will compute the decay widths for both UV regulators, and the spread of results will account for this source of uncertainty.

[9] There appear small differences in the central value of the resonance mass with respect to value quoted in [15] due to small differences in the used hadron masses.

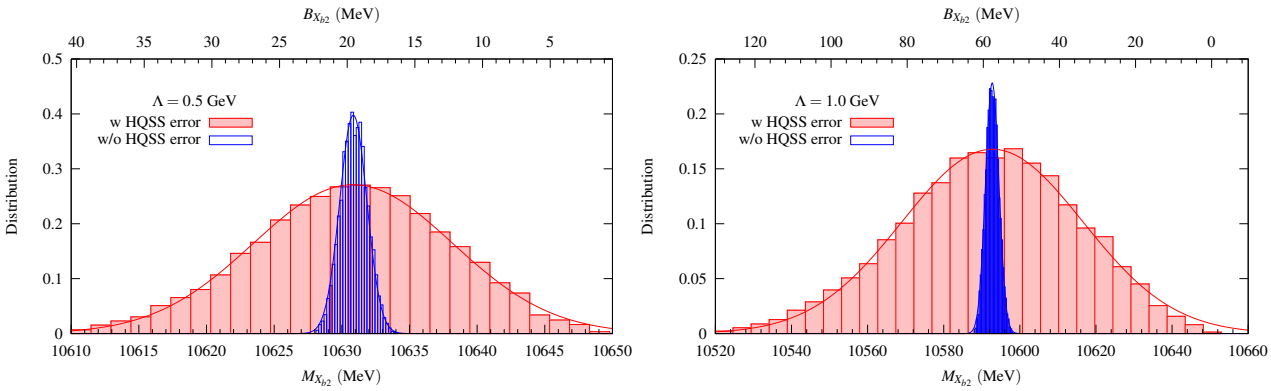

FIG. 2. Same as in Fig. 1 but in the bottom sector. To better appreciate the distribution details, the $\Lambda = 0.5$ (1) GeV red histogram, which includes the 20% HQSS error, has been multiplied by a factor of 5 (10).

III. THE HADRONIC X_2 AND X_{b2} DECAYS

The quantum numbers, $J^{PC} = 2^{++}$, of these resonances constrain their possible decay channels. In this work, for hadronic decays we only consider the decays into two heavy hadrons: $X_2 \to D\bar{D}$ and $X_2 \to D\bar{D}^*(D^*\bar{D})$, and the analogous processes $X_{b2} \to B\bar{B}$ and $X_{b2} \to B\bar{B}^*(B^*\bar{B})$. We expect that these d-wave decay modes should largely saturate the widths of these states. Because the $D\bar{D}$ couples in a d-wave to the 2^{++} system, its contribution to the mass renormalization of the X_2 is of higher order (see Appendix B). We thus did not include the $D\bar{D}$ as a coupled channel in the T-matrix, but treat it perturbatively. This means that the transitions are mediated by the exchange of a pion. The relevant $\pi P^{(*)} P^{(*)}$ vertices are taken from the LO Lagrangian of heavy meson chiral perturbation theory [40–43] (see Appendix A 2). At LO, besides the pion decay constant, $f_\pi = 92.2$ MeV, there appears only one additional $D^* D\pi$ coupling (g). We take $g = 0.570 \pm 0.006$ as inferred from the new value of $\Gamma = (83.4 \pm 1.8)$ keV for the D^{*+} decay width quoted by the PDG [5]. This is mostly determined by the recent BABAR Collaboration measurement [44] of this width, which is approximately a factor 12 times more precise than the previous value, $\Gamma = (96 \pm 4 \pm 22)$ keV by the CLEO Collaboration [45]. Thus, we end up with an uncertainty of the order 1% for g. Though the hadronic X_2 and X_{b2} widths evaluated in this section will be proportional to g^4, this source of error ($\sim 4\%$) will be much smaller than others and it will be ignored in what follows.

	without pion-exchange FF		with pion-exchange FF	
	$\Lambda = 0.5$ GeV	$\Lambda = 1$ GeV	$\Lambda = 0.5$ GeV	$\Lambda = 1$ GeV
$\Gamma(X_2 \to D^+D^-)$ [MeV]	$3.3^{+3.4}_{-1.4}$	$7.3^{+7.9}_{-2.1}$	$0.5^{+0.5}_{-0.2}$	$0.8^{+0.7}_{-0.2}$
$\Gamma(X_2 \to D^0\bar{D}^0)$ [MeV]	$2.7^{+3.1}_{-1.2}$	$5.7^{+7.8}_{-1.8}$	$0.4^{+0.5}_{-0.2}$	$0.6^{+0.7}_{-0.2}$
$\Gamma(X_2 \to D^+D^{*-})$ [MeV]	$2.4^{+2.1}_{-1.0}$	$4.4^{+3.1}_{-1.2}$	$0.7^{+0.6}_{-0.3}$	$1.0^{+0.5}_{-0.2}$
$\Gamma(X_2 \to D^0\bar{D}^{*0})$ [MeV]	$2.0^{+2.1}_{-0.9}$	$3.5^{+3.5}_{-1.0}$	$0.5^{+0.6}_{-0.2}$	$0.7^{+0.5}_{-0.2}$

TABLE I. $X_2(4013) \to D\bar{D}, D\bar{D}^*$ decay widths using different UV Gaussian regulators for the $D^*\bar{D}^*X_2$ form factor and with/without including a pion-exchange vertex form factor (FF) in each of the $D^*D\pi$ and $D^*D^*\pi$ vertices in the three-point loop function. The decay widths of the $X_2(4013) \to \bar{D}D^*$ modes are the same thanks to C-parity. Uncertainties are obtained from a Monte Carlo simulation using the X_2 binding energy histograms displayed in Fig. 1 (red shaded) and the $g_0^{X_2}$ and $g_c^{X_2}$ couplings given in Eqs. (10) and (11). Note that the procedure takes into account 20% HQSS uncertainties and the correlations between X_2 masses (binding energies) and $g_0^{X_2}$ and $g_c^{X_2}$ couplings. Errors on the widths provide 68% CL intervals.

A. Charm decays

1. $X_2(4013) \to D\bar{D}$

We will first consider the $X_2(4013) \to D^+D^-(D^0\bar{D}^0)$ decay, which proceeds through the Feynman diagrams depicted in Fig. 3. We treat charm mesons non-relativistically, and neglect $p_{D^*,\bar{D}^*}/m_{D^*}$ terms and the temporal components in the $D^*, \bar{D}^*$ propagators. We obtain for the $X_2(4013) \to D^+D^-$ process, in the resonance rest frame and with q and k the 4-momenta of the D and $\bar{D}$ final mesons ($\vec{q} = -\vec{k}$, $q^0 + k^0 = M_{X_2}$),

$$
\begin{aligned}
&-i\,\mathcal{T}(\lambda)_{D^+D^-} \\
&= -\frac{Ng^2}{f_\pi^2}\epsilon_{ij}(\lambda)\left\{ g_c^{X_2}\int \frac{d^4l}{(2\pi)^4}\frac{l^i\,l^j}{\left[(l+q)^2 - m_{D^{*+}}^2 + i\varepsilon\right]\left[(k-l)^2 - m_{D^{*-}}^2 + i\varepsilon\right]\left(l^2 - m_{\pi^0}^2 + i\varepsilon\right)}\right. \\
&\left. +2g_0^{X_2}\int \frac{d^4l}{(2\pi)^4}\frac{l^i\,l^j}{\left[(l+q)^2 - m_{D^{*0}}^2 + i\varepsilon\right]\left[(k-l)^2 - m_{\bar{D}^{*0}}^2 + i\varepsilon\right]\left(l^2 - m_{\pi^-}^2 + i\varepsilon\right)}\right\} \\
&= i\frac{Ng^2}{f_\pi^2}\epsilon_{ij}(\lambda)\left\{ g_c^{X_2} I^{ij}(m_{D^{*+}}, m_{\pi^0}; M_{X_2}, q^\mu) + 2g_0^{X_2} I^{ij}(m_{D^{*0}}, m_{\pi^-}; M_{X_2}, q^\mu)\right\},
\end{aligned}
\tag{13}
$$

where $\epsilon_{ij}(\lambda)$ is the symmetric spin-2 tensor with λ denoting the polarization of the X_2 state[10] and $N = \sqrt{8M_{X_2}m_{D^*}^2}\left(\sqrt{m_D m_{D^*}}\right)^2$ accounts for the normalization of the heavy meson fields[11] and some

[10] For instance, it could be given by

$$\epsilon_{ij}(\lambda) = \sum_{\lambda_1,\lambda_2}(1,1,2|\lambda_1,\lambda_2,\lambda)\epsilon^i_{\lambda_1}\epsilon^j_{\lambda_2}$$

with $\epsilon^i_0 = (0,0,1)$, and $\epsilon^i_{\pm 1} = \mp(1,\pm i,0)/\sqrt{2}$, and $(j_1,j_2,j|m_1,m_2,m)$ a Clebsch-Gordan coefficient.

[11] We use a non-relativistic normalization for the heavy mesons, which differs from the traditional relativistic one by a factor $\sqrt{M_H}$.

additional factors needed when the couplings $g_{c,0}^{X_2}$, as determined from the residues at the pole of the EFT T-matrix, are used for the $X_2 D^* \bar{D}^*$ vertex. For the neutral and charged pion masses, we have used the values quoted by the PDG [5] and heavy meson isospin averaged masses to compute N. Besides, I^{ij} is a three-point loop function, the detailed evaluation of which is relegated to the Appendix C 1.[12] The loop is seemingly logarithmically divergent. However, since the X_2 polarization is traceless, the divergent part which comes with a Kronecker delta does not contribute. This is because the decay occurs in a d-wave, thus the loop momentum is converted to external momenta, and the remaining part of the integral is convergent. Nevertheless, we will include two different form factors in the computation of the three-point loop function. One is inherited from the UV regularization/renormalization procedure sketched in Eq. (5) and employed to make the LSE T-matrix finite. In addition, we will include a second form factor to account for the large virtuality of the pion in the loop. We will discuss this at length below and in Appendix C 1.

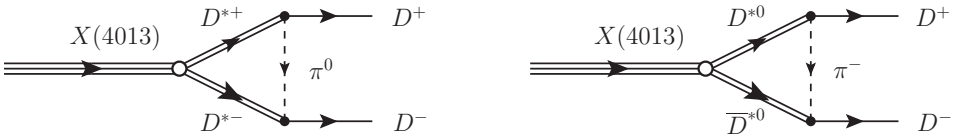

FIG. 3. Feynman diagrams for the $X_2(4013) \to D^+ D^-$ decay. Diagrams for the $X_2(4013) \to D^0 \bar{D}^0$ transition are similar, with the appropriate changes of the exchanged pion charges.

Analogously, the $X_2(4013) \to D^0 \bar{D}^0$ amplitude is,

$$-i\,\mathcal{T}(\lambda)_{D^0\bar{D}^0} = i\frac{N g^2}{f_\pi^2}\epsilon_{ij}(\lambda)\left\{2 g_c^{X_2} I^{ij}(m_{D^{*+}}, m_{\pi^+}; M_{X_2}, q^\mu) + g_0^{X_2} I^{ij}(m_{D^{*0}}, m_{\pi^0}; M_{X_2}, q^\mu)\right\}. \quad (14)$$

The two-body decay width in the X_2 rest-frame reads [5]:

$$\frac{d\Gamma_a}{d\Omega(\hat{q})} = \frac{1}{5}\sum_\lambda |\mathcal{T}(\lambda)_a|^2 \frac{|\vec{q}|}{32\pi^2 M_{X_2}^2}, \qquad a = D^+D^-,\ D^0\bar{D}^0\ . \quad (15)$$

The sum over the X_2 polarizations can be easily done in the c.m. frame,

$$\sum_\lambda \epsilon_{mn}(\lambda)\epsilon_{ij}^*(\lambda) = \frac{1}{2}\left[\delta_{mi}\delta_{nj} + \delta_{ni}\delta_{mj} - \frac{2}{3}\delta_{mn}\delta_{ij}\right], \quad m,n,i,j = 1,2,3\ . \quad (16)$$

As discussed in Appendix C 1, the three-point loop function has a tensor structure of the type

$$I^{ij}(\vec{q}) = I_0(\vec{q}^{\,2})\, q^i q^j + I_1(\vec{q}^{\,2})\,\delta^{ij}\,|\vec{q}|^2\ . \quad (17)$$

[12] In the computation of I^{ij}, we are consistent with the former approximations, and we use non-relativistic charm meson propagators.

The I_1 term carries the UV divergence, which however does not contribute to the width, because it vanishes after the contraction with the traceless spin-2 polarization tensor, as mentioned above. Therefore, only the I_0 term is relevant, which is free of UV divergences. Moreover, the contraction of $I^{ij}(\vec{q})\, I^{mn}(\vec{q})$ with $\sum_\lambda \epsilon_{mn}(\lambda)\epsilon^*_{ij}(\lambda)$ [Eq. (16)] leads to a factor of $2\vec{q}^{\,4}/3$. Thus, the integration over the solid angle $d\Omega(\hat{q})$ trivially gives 4π, and the width scales like $|\vec{q}|^5$ as expected for a d-wave process.

Our predictions for the $X_2(4013) \to D^+D^-, D^0\bar{D}^0$ decays are compiled in Table I. If we look at the first two columns of results in the table, we find widths of the order of a few MeV, with asymmetric errors that favour larger values. This is mostly due to the similar asymmetry of the uncertainties quoted for the $g_0^{X_2}$ and $g_c^{X_2}$ couplings in Eqs. (10) and (11).

Our scheme is based on a low-energy EFT, in which the momenta should be smaller than a hard scale which serves as a momentum cutoff [see Eq. (5)]. The high-momentum modes are out of control in the low-energy EFT. Therefore in the computation of the width, we include a Gaussian regulator at the $D^*\bar{D}^*X_2$ vertex, as discussed in Eq. (C6). The cutoff should be the same as the one used in generating the X_2 as it is related to the same unitary cut in the $D^*\bar{D}^*$ system. In Fig. 4, we display, as an example, the dependence of the $I_0(m_{D^{*0}}, m_{\pi^0}; M_{X_2}, q^\mu[m_{F_1} = m_{F_2} = m_{D^0}])$ integrand [see Eqs. (C5)-(C7)] on the pion loop momentum. In the left plot we see that in spite of including the Gaussian X_2 form factor, large momenta above 1 GeV provide a sizable contribution to the integral ($\simeq 14\%$, 30% and 45% for $\Lambda = 0.5$ GeV, 1 GeV and ∞, respectively), which is an unwanted feature within the low-energy EFT scheme and signals a sizeable short-distance contribution. Indeed, the momentum of the exchanged pion, peaks at around 750 MeV, which is a somehow large value in the sense that the hard scale for the chiral expansion which controls the pionic coupling is $\Lambda_\chi \sim 1$ GeV. We see that below the peak, the curves for both cutoff values are very close to each other, and they are also close to the curve corresponding to the case without any regulator. This is the region where the low-energy expansion works and thus model-independent conclusions can be made. The curves start deviating from each another after the peak, that is in the region with a pion momentum $\gtrsim \Lambda_\chi$. Because the loop integrals are not completely dominated by momentum modes well below Λ_χ, the widths of interest will bear an appreciable systematic uncertainty. This is reflected in the fact that the widths in the second column in Table I are larger than those in the first column by a factor around 2.[13]

On the other hand, the fact that the pion could be quite far off-shell should be reflected in the $D^*D\pi$ vertex, which should be corrected, similarly as it is done in the case of the $NN\pi$ one. Thus,

[13] Note that the coupling constants obtained with both cutoffs are similar, see Eqs. (10) and (11), and thus the difference should come mainly from the loop integration.

to give an estimate of the hadronic decay widths, in the spirit of the Bonn potential [46], we have included a monopole pion-exchange vertex form factor, with a hadron scale of the order of 1 GeV, in each of the $D^*D\pi$ vertices [Eq. (C7)]. Its effect on the internal pion momentum dependence of the $I_0(m_{D^{*0}}, m_{\pi^0}; M_{X_2}, q^\mu[m_{F_1} = m_{F_2} = m_{D^0}])$ integrand is shown in the right plot of Fig. 4. The large pion momenta contribution ($|\vec{l}\,| > 1$ GeV), which is not reliable in a low-energy EFT calculation, is reduced now to 6.5%, 13% and 16% for $\Lambda = 0.5$ GeV, 1 GeV and ∞, respectively. This makes also more appropriate the non-relativistic treatment of the charmed mesons adopted here. Besides, the dependence of the width on the UV Gaussian regulator is significantly softer, though the widths are further reduced by almost an order of magnitude.

We believe that the most realistic estimates are those obtained with the inclusion of the pion-exchange form factor and the spread of results compiled in Table I give a conservative estimate of the systematic uncertainties, beyond the mere existence of the $X_2(4013)$ state, as discussed in Sect. II B. We remind here that because of the additional 20% HQSS uncertainty, approximately a 23% (32%) for $\Lambda = 0.5$ GeV ($\Lambda = 1$ GeV) of the $X(3872)$ events [$(M_{X(3872)}, R_{X(3872)})$ MC samples] do not produce the X_2 as a bound state pole, since the strength of the resulting interaction in the 2^{++} sector is not attractive enough to bind the $D^*\bar{D}^*$.

Nevertheless, assuming the existence of the X_2 state, and in view of the results given in Table I, we estimate the $X_2 \to D\bar{D}$ partial width (including both the charged and neutral channels) to be

$$\Gamma(X_2 \to D\bar{D}) = \left(1.2 \pm \underbrace{0.3}_{\text{sys}\,(\Lambda)} \,^{+1.3}_{-0.4}\right) \text{ MeV}, \tag{18}$$

where the first error accounts for the dependence on the UV Gaussian regulator used in the $D^*\bar{D}^*X_2$ vertex, while the second one is obtained from the uncertainties given in Table I. This latter error includes both some additional systematic (HQSS violations) and statistical ($X(3872)$ input used to fix the properties of the X_2 resonance) uncertainties. Notice that, as discussed above, the calculation is probably already beyond the valid range of the EFT due to the large contribution of high-momentum modes. We thus have adopted a more phenomenological strategy and used the pion-exchange form factor with a cutoff of 1 GeV to make an estimate of the decay widths. The values presented in Eq. (18) refer only to the last two columns in Table I that include the effect of the pion-exchange form factor. Thus, and considering both sets of errors, we cover the range 0.5–2.8 MeV, which accounts for all values including errors quoted in the table.

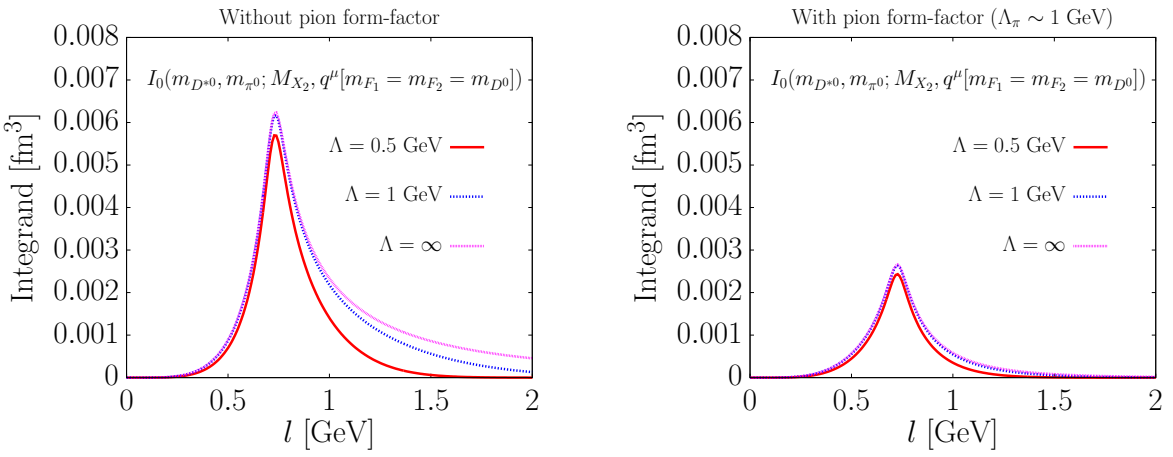

FIG. 4. Dependence of the $I_0(m_{D^{*0}}, m_{\pi^0}; M_{X_2}, q^\mu[m_{F_1} = m_{F_2} = m_{D^0}])$ integrand [see Eqs. (C5)-(C7)] on the pion loop momentum $|\vec{l}|$. For the X_2 mass we have used 4013 MeV. Results with and without the inclusion of the pion form factor [Eq. (C7)] squared are presented in the right and left plots, respectively. In both cases, three different choices of the Gaussian regulator [Eq. (C6)] in the $D^*\bar{D}^*X_2$ vertex have been considered.

2. $X_2(4013) \to D\bar{D}^*(D^*\bar{D})$

Here, we will study the D^+D^{*-}, and $D^0\bar{D}^{*0}$ channels, which proceeds through the Feynman diagrams depicted in Fig. 5. This is also a d-wave decay so that both angular momentum and parity are conserved. The decay widths are expected to be comparable to those found for the $X_2(4013) \to D\bar{D}$ decays, despite the phase space is considerably more reduced. This extra enhancement is caused by the extra multiplicity due to the spin of the final $D^*(\bar{D}^*)$ meson.

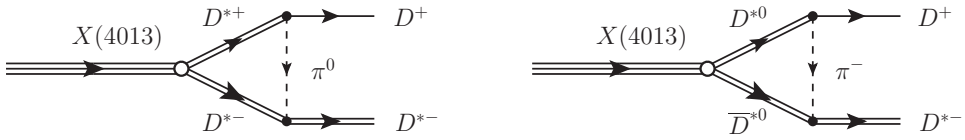

FIG. 5. Feynman diagrams for the $X_2(4013) \to D^+D^{*-}$ decay. Diagrams for the $X_2(4013) \to D^0\bar{D}^{*0}$ transition are similar, with the appropriate changes of the exchanged pion charges.

As commented before, we treat charm mesons non-relativistically and obtain the decay amplitude for the $X_2(4013) \to D^+D^{*-}$ process as

$$\mathcal{T}(\lambda, \lambda_*)_{D^+D^{*-}} = i\frac{N^* g^2}{f_\pi^2}\epsilon_{ij}(\lambda)\epsilon_{mnj}\epsilon^{*n}(\lambda_*)\Big\{g_c^{X_2} I^{im}(m_{D^{*+}}, m_{\pi^0}; M_{X_2}, q^\mu) + 2g_0^{X_2} I^{im}(m_{D^{*0}}, m_{\pi^-}; M_{X_2}, q^\mu)\Big\}\,, \tag{19}$$

in the resonance rest frame. Here, q is the 4-momenta of the D^+ meson, and $\epsilon^n(\lambda^*)$ is the polarization

vector of the final D^{*-} meson with helicity λ_*, $N^* = \sqrt{8M_{X_2}m_{D^*}^2}\sqrt{m_D m_{D^*}^3}$ and ϵ_{imn} is the 3-dimensional Levi-Civita antisymmetric tensor. Analogously, the $X_2(4013) \to D^0\bar{D}^{*0}$ amplitude is,

$$\mathcal{T}(\lambda,\lambda_*)_{D^0D^{*0}} = i\frac{N^* g^2}{f_\pi^2}\epsilon_{ij}(\lambda)\epsilon_{mnj}\epsilon^{*n}(\lambda_*)\Big\{2g_c^{X_2} I^{im}(m_{D^{*+}}, m_{\pi^+}; M_{X_2}, q^\mu) + g_0^{X_2} I^{im}(m_{D^{*0}}, m_{\pi^0}; M_{X_2}, q^\mu)\Big\}. \tag{20}$$

The two-body decay width in the X_2 rest-frame in this case reads [5]:

$$\frac{d\Gamma_a}{d\Omega(\hat{q})} = \frac{1}{5}\sum_{\lambda,\lambda_*}|\mathcal{T}(\lambda,\lambda_*)_a|^2\frac{|\vec{q}|}{32\pi^2 M_{X_2}^2}, \qquad a = D^+D^{*-}, D^0\bar{D}^{*0}\ . \tag{21}$$

The sum over the $\bar{D}^*$ and X_2 polarizations can be easily done, and we get

$$\sum_\lambda \epsilon_{ij}(\lambda)\epsilon^*_{rs}(\lambda)\sum_{\lambda_*}\epsilon^{*n}(\lambda_*)\epsilon^p(\lambda_*)\epsilon_{mnj}\epsilon_{lps} = \frac{1}{6}\left[7\delta_{ml}\delta_{ir} + 2\delta_{il}\delta_{rm} - 3\delta_{lr}\delta_{mi}\right], \quad i,l,m,r = 1,2,3\ . \tag{22}$$

The above tensor structure should be contracted with $I^{im}(\vec{q})\, I^{rl}(\vec{q})$. We see that the sum over polarizations of Eq. (22) is orthogonal to δ_{im} and δ_{rl}, which guarantees also here that only the UV finite I_0 term of the three-point loop function is relevant. The contraction leads to a $\vec{q}^4$ factor,[14] and thus the width scales like $|\vec{q}|^5$, as expected for a d-wave decay.

Results for the $X_2 \to D\bar{D}^*$ decay widths are also compiled in Table I. We only show predictions for the $X_2(4013) \to D^+D^{*-}(D^0\bar{D}^{*0})$ decays, because being the X_2 an even C-parity state, its decay modes into the charge conjugated final states have the same decay widths. In what respects to the effect of the form factors, the discussion runs in parallel to that in the Sect. III A 1, though the effect of the pion-exchange form factor is significantly smaller here (a factor 4 or 5 at most). As expected, the widths are comparable to those found for the $X_2 \to D\bar{D}$ decays. Finally, we estimate the partial $X_2 \to D\bar{D}^*\,(D^*\bar{D})$ width (including both the charged and neutral channels as well as the charge-conjugated modes) to be

$$\Gamma(X_2 \to D\bar{D}^*) + \Gamma(X_2 \to D^*\bar{D}) = \big(2.9 \pm \underbrace{0.5}_{\text{sys}\,(\Lambda)}\,{}^{+2.0}_{-1.0}\big)\ \text{MeV}, \tag{24}$$

where the errors have been estimated as in Eq. (18). The above result, together with that obtained previously for the $D\bar{D}$ channel, leads to a total X_2 width of the order of 2-8 MeV, assuming its existence.

[14] In the $D\bar{D}$ mode, studied in Sect. III A 1 a factor of $2\vec{q}^4/3$ is obtained instead. Thus, neglecting the $D - D^*$ mass difference, because the loop integrals are the same, we would find

$$|\mathcal{T}_{D\bar{D}^*(D^*\bar{D})}|^2 \simeq \frac{3}{2}|\mathcal{T}_{D\bar{D}}|^2 \tag{23}$$

This extra factor 3/2 due to the spin-1 polarization vector produces an enhancement of the $D\bar{D}^*$ decay mode with respect to the $D\bar{D}$ one, which partially compensates the smaller available phase space.

	FFπ1 FFX_2-G	FFπ2 FFX_2-G	FFπ1 FFX_2-L	FFπ2 FFX_2-L	FFπ1 FFX_2-G	FFπ2 FFX_2-G	FFπ1 FFX_2-L	FFπ2 FFX_2-L
Λ [GeV]	0.5	0.5	0.4	0.4	1	1	0.8	0.8
$\Gamma(X_2 \to D^+D^-)$	$0.5^{+0.5}_{-0.2}$	0.6	0.5	0.6	$0.8^{+0.7}_{-0.2}$	01.0	0.9	0.9
$\Gamma(X_2 \to D^0\bar{D}^0)$	$0.4^{+0.5}_{-0.2}$	0.5	0.4	0.4	$0.6^{+0.7}_{-0.2}$	0.7	0.6	0.6
$\Gamma(X_2 \to D^+D^{*-})$	$0.7^{+0.6}_{-0.3}$	0.9 (1.2)	0.7	0.8 (1.1)	$1.0^{+0.5}_{-0.2}$	1.2 (1.6)	1.0	1.1 (1.5)
$\Gamma(X_2 \to D^0\bar{D}^{*0})$	$0.5^{+0.6}_{-0.2}$	0.7 (0.9)	0.5	0.6 (0.8)	$0.7^{+0.5}_{-0.2}$	0.8 (1.2)	0.7	0.8 (1.1)

TABLE II. $X_2(4013) \to D\bar{D}, D\bar{D}^*$ decay widths (in MeV units) using different UV regularization schemes for the $D^*\bar{D}^*X_2$ vertex and pion-exchange form factors. FFX_2-G and FFX_2-L stand for the results obtained with Gaussian (Eq. (5)) and Lorentzian (Eq. (26)) regularized local interactions, respectively. On the other hand, the widths in the columns FFπ1 and FFπ2 were obtained inserting the pion form factor of Eq. (C7) and $F(\vec{l}^{\,2}, \Lambda_\pi) = e^{-\vec{l}^{\,2}/\Lambda_\pi^2}$ in each of the two $D^*D^{(*)}\pi$ vertices, respectively. In the latter case, we take $\Lambda_\pi = 1.2$ GeV, as determined in the QCDSR calculation of Ref. [49] for the $D^*D\pi$ coupling. In the $D\bar{D}^*$ decay mode, we also show results (in brackets) obtained when a larger cutoff, $\Lambda_\pi = 1.85$ GeV, is used in the $D^*D^*\pi$ vertex, as obtained in the QCDSR study carried out in Ref. [50] for this coupling. The results presented in Table I correspond to the [FFX_2-G & FFπ1] columns and for the rest of choices we only provide central values.

3. *Charm decays: further analysis of uncertainties*

The uncertainties on the results compiled in Table I account both for reasonable estimates of HQSS corrections, as well as for the statistical errors on the inputs used to fix the LEC's that determine the properties (mass and $D^*\bar{D}^*$ couplings) of the X_2 resonance. Moreover we are using an EFT to describe these decays, which means that there is an intrinsic uncertainty that can be determined systematically. We indicated the size of this error in Eqs. (18) and (24). For obtaining the EFT uncertainty we combined the predictions obtained for two different UV Gaussian cutoffs ($\Lambda = 0.5$ and 1 GeV) in the $D^*\bar{D}^*X_2$ vertex, and used the spread of values to quantify this error. The idea is that the residual dependence of the results on the cutoff should provide an insight into the size of sub-leading corrections.

Now, we try to further test the robustness of the systematic errors quoted in Eqs. (18) and (24). To that end, we have examined:

- The dependence of our results on the functional form of the UV regulators, both in the $D^*\bar{D}^*X_2$ and $D^*D^{(*)}\pi$ vertices.

  - We have a contact theory with a Gaussian regulator and a cutoff Λ between 0.5 and 1

GeV. This theory, though very simple, is the LO of an EFT expansion describing the low energy dynamics of heavy hadrons (see Ref. [36] for details). Within the EFT we can expand observable quantities as a power series of the type

$$A = \sum_{\nu} \hat{A}_\nu \left(\frac{p}{\Lambda_M} \right)^\nu , \tag{25}$$

where p is the momenta of the hadrons and Λ_M the scale at which hadrons stop behaving as point-like particles (about the ρ mass). A LO calculation only keeps the first term in the series above. Hence it should have a relative error of order (p/Λ_M). We stress that this is expected to be so regardless of the exact regulator employed (gaussian, lorentzian, etc.), provided that the cutoff is at least of the order of Λ_M. The reason for that is that the calculations we show are renormalizable: once the counter-terms are fixed[15], they only contain negative powers of the cutoff Λ when we expand on the large cutoff limit. Hence, the uncertainty in the calculation is of order (p/Λ). By taking Λ of the order of Λ_M, observables are guaranteed to have a cutoff uncertainty of the order (p/Λ_M), equivalent to the EFT uncertainty.

There are several methods for making a more precise estimation of the EFT error: the one we use in Table I is to vary the cutoff around values of the order of Λ_M (hence the choice of the $0.5 - 1\,\text{GeV}$ cut-off window). EFT predictions for two different cutoffs differ by a factor of (p/Λ_M) and that is why we chose this particular way of assessing the errors.

Alternatively, one could use different regulators or form factors to assess the size of this error. This idea also gives a cross-check of the previous error estimates based on varying the cut-off. We have employed a different regulator to check that our former estimation of the EFT errors is correct and to show that the particular regulator employed is not important. We closely follow here the discussion of Sect. VII of Ref. [37] and consider a Lorentz form for the regulator

$$\langle \vec{p}\,|V|\vec{p}\,'\rangle = C_{IX} \left[\frac{\Lambda^2}{\Lambda^2 + \vec{p}^{\,2}} \right] \left[\frac{\Lambda^2}{\Lambda^2 + \vec{p}^{\,\prime 2}} \right] , \tag{26}$$

with two values of the cutoff, namely $\Lambda = 0.4$ and 0.8 GeV, which were obtained by multiplying the Gaussian cutoffs by a factor of $\sqrt{2/\pi}$ [37]. The resulting[16] widths are presented in Table II and turn out to be rather insensitive to the form of the regulator (this is to be understood within the limits of the expected EFT uncertainty).

[15] See for instance the discussion of Eqs. (23) and (24) of Ref. [37].

[16] With the Lorentzian regularized local potential, we re-obtain the counter-terms C_{0X} and C_{1X} from the $X(3872)$ inputs, which are then used to find the mass of the X_2 resonance and its couplings to the $D^{*0}\bar{D}^{*0}$ and $D^{*-}D^{*+}$ meson pairs. These physical quantities hardly change, because the X_2 is a very loosely bound state and its dynamics is very little sensitive to the details of the $D^*\bar{D}^*$ interaction at short distances.

– Next we have studied the dependence of the widths on the pion form factor that accounts for the off-shellness of the pion in the mechanisms depicted in Figs. 3 and 5. To that end we used the results from the QCD sum rule (QCDSR) calculations performed in Refs. [49, 50]. The first of these two works considers the $D^*D\pi$ vertex: it was found the form factor is harder if the off-shell meson is heavy, implying that the size of the vertex depends on the exchanged meson. This means that a heavy meson will see the vertex as point-like, whereas the pion will see its extension. The authors of Ref. [49] find an on-shell value $g = 0.48 \pm 0.05$ (note the different definition used in this reference), around 1-2 sigmas below the value of 0.57 used in this work. In addition, they adjust their results for off-shell pions to a Gaussian form e^{l^2/Λ_π^2}, with l^μ the pion four momentum, and find $\Lambda_\pi = 1.2$ GeV. This form-factor[17], in the region of interest for this work, turns out to be in a good agreement with that used to obtain the results presented in Table I. This can be seen in the new results showed in Table II and obtained with this new pion off-shell form-factor (FFπ2). Deviations from our previous estimates of the $X_2(4013) \to D\bar{D}, D\bar{D}^*$ decay widths are both much smaller than the (HQSS & exp) uncertainties quoted in Table I, and well comprised within the systematic uncertainty generated when the $D^*\bar{D}^*X_2$ cutoff varies in the 0.5-1 GeV window.

In the $X_2 \to D\bar{D}^*$ decay, there also appears the $D^*D^*\pi$ coupling in one of the vertices, see Fig. 5. The off-shell behavior of this vertex might differ from that of the $D^*D\pi$ one. This coupling was studied using QCDSR in [50] where, translating the definition used therein to the one used here, it was found an on-shell value $g = 0.56 \pm 0.07$ in good agreement with the HQSS expectations. The off-shell behavior was described by a Gaussian, as in the case of the $D^*D\pi$ vertex, but with a significantly larger cutoff, Λ_π= 1.85 GeV. This significant difference is somehow surprising from the HQSS point of view, and we should note that the QCDSR actual calculations in [50] were carried out for significantly larger values of $l^2 > 4$ GeV^2 than in the case of the $D^*D\pi$ coupling analyzed in Ref. [49]. Nevertheless, we used this softer dependence for the $D^*D^*\pi$ vertex and re-computed the $D\bar{D}^*$ widths. Results are shown in brackets in Table II. Changes are now larger, and in general are of the order of 50%, though they could be still accommodated within the HQSS and EFT uncertainties already considered in our original calculations. The large momenta of the external mesons, that can even exceed

[17] To use the form factor of Ref. [49] in the computation of the widths, we have approximated the pion four momentum squared by $-\vec{l}^2$, which is sufficiently accurate because the dominant part of the integration comes from regions where the two virtual D^* and $\bar{D}^*$ mesons are almost on-shell. In this region, the energy of both heavy light vector mesons is approximately $M_{X_2}/2$ which coincides with that of the external heavy mesons, and hence l^0 is much smaller than $|\vec{l}|$.

0.5 GeV, make it possible that the short distance details of the decay mechanisms could be relevant. This is the weakest point in our scheme. The reason is that the EFT uncertainty is expected to be 0.5 GeV$/\Lambda_M \gtrsim 1/2$, as the variations of the $D\bar{D}^*$ widths in Table II seem to confirm, and the calculation is really on the limit of validity of this kind of description and should only be considered as a reasonable estimate.

- The contribution of decay mechanisms driven by the exchange of shorter range mesons (heavier) than the pion.

  Since the momenta of the external charmed mesons can exceed 0.5 GeV, one might think that shorter range contributions such as the ρ and ω exchanges could be sizable, and even comparable to those of the diagrams depicted in Figs. 3 and 5 for the exchange of a pion. We will focus on the $X_2 \to D\bar{D}$ decay mode, where the momenta of the external mesons is the largest and we will begin by studying the effects of the exchange of a ρ meson. If we use the phenomenological $D^*D\rho$ Lagrangian given in Eq. (3e) of Ref. [51], we find that the amplitudes of this new contribution can be obtained from those driven by pion exchange, and given in Eqs. (13) and (14), by replacing m_{π^0} and m_{π^+} by m_{ρ^0} and m_{ρ^+} in the loop integrals and

$$\frac{g^2}{f_\pi^2} \to -\frac{m_D}{m_{D^*}} g^2_{D^*D\rho} \tag{27}$$

  where we have neglected $|\vec{q}|^2/m^2_{D^{(*)}}$ terms, with $\vec{q}$ the c.m. three-momentum of the external D and $\bar{D}$ mesons. The coupling constant $g_{D^*D\rho}$ has been computed in various schemes [51–55] (ordinary and light cone QCDSR, vector dominance model, SU(4), etc.) and it varies in the range $[2.8 \pm 0.1, 4.3 \pm 0.9]$ GeV^{-1} (see Table 5 of Ref. [55]). Taking $g_{D^*D\rho} \sim 5$ GeV^{-1}, in the highest part of the interval of calculated values, we would have $g^2_{D^*D\rho}/(g^2/f_\pi^2) \sim 2/3$, while a direct calculation of the loop integrals shows that those calculated using the ρ mass instead of the pion mass are around a factor of two smaller. Altogether, this indicates that the absolute values of the ρ-exchange amplitudes are about a factor of three smaller than those driven by the pion exchange. If one uses $g_{D^*D\rho} \sim 3$ GeV^{-1}, now in the lowest part of the interval of values, the ρ contribution will be, at the level of amplitudes, around eight times smaller than those considered in the present work. In any case, these effects are smaller than the HQSS and EFT uncertainties quoted in Table I, and therefore it seems justified to neglect them. On the other hand, the ω-exchange contributions are even smaller, around a factor of three, because this meson is neutral, and it cannot generate mechanisms where a light charged meson is exchanged.

To estimate the size of the ρ exchange contribution in the $X_2 \to D\bar{D}^*$ decay mode, in addition to the $D^*D\rho$ vertex, we have used the phenomenological $D^*D^*\rho$ Lagrangian given in Eq. (1f) of Ref. [51]. The amplitudes of this new mechanism can be obtained from those driven by pion exchange, and given in Eqs. (19) and (20), by replacing m_{π^0} and m_{π^+} by m_{ρ^0} and m_{ρ^+}, and $P_2(x) \to (P_2(x) + x|\vec{q}|/l)$ in the computation of the loop integral I_0 (see Eq. (C5) of Appendix C 1) and using the appropriate coupling constants

$$\frac{g^2}{f_\pi^2} \to \sqrt{\frac{m_D}{m_{D^*}}} g_{D^*D\rho} \frac{g_{D^*D^*\rho}}{m_{D^*}} \tag{28}$$

where we have neglected as before the $|\vec{q}|^2/m^2_{D^{(*)}}$ terms. (At this point, the phase in Eq. (28) is arbitrary, because the phase convention used in [51] and in this work for the heavy meson fields is different.) The $g_{D^*D^*\rho}$ coupling is set to 2.52 in [51], while it is estimated to be 4.7 ± 0.2 in [53, 56] (QCDSR). On the other hand, there exist some partial cancellations in the loop integral in this case, and it turns out to be at least a factor of 5 smaller than that calculated for the pion driven contribution. Thus, and having in mind the previous discussion for the expected range of values of the $g_{D^*D\rho}$ coupling, we conclude that the $\rho-$exchange contribution can be safely neglected in the $X_2 \to D\bar{D}^*$ decay mode.

In view of the results discussed in this subsection, we should acknowledge that as a result of the contribution from highly virtual pions, which is certainly in the limit of applicability of the low-energy EFT, the hadronic decay widths bear a large systematic uncertainty. Nevertheless, we have given arguments to be reasonably convinced that the results quoted in Eqs. (18) and (24) provide sensible estimates for the $X_2(4013) \to D\bar{D}, D\bar{D}^*$ widths.

In the next subsection, we will study these hadronic decays in the bottom sector. There, the considerations are parallel to those discussed here for the charm sector.

B. Bottom decays

Thanks to the heavy flavor symmetry, the results of the previous subsection can be trivially extended to the bottom sector. There, we have a robust prediction, even when HQSS uncertainties (20%) are taken into account, for the X_{b2} resonance (see Fig. 2). Moreover, all sort of non-relativistic approximations adopted in the current scheme are now more suited, since the range of variation of the internal pion momentum in the loops is similar to that shown in Fig. 4 for the charm sector.

On the other hand, as discussed in Sect. II C, we do not expect any significant isospin breaking effects and the X_{b2} resonance would be a pure $I = 0$ state, with equal coupling to its neutral and

charged components. For simplicity, we will also neglect the tiny difference between B^0 and $B^\pm$ masses, and we will use a common mass $m_B = (m_{B^0} + m_{B^\pm})/2 = 5279.42$ MeV. Yet, for the pion mass that appears in the loop integral, we take the isospin averaged value $m_\pi = (2m_{\pi^\pm} + m_{\pi^0})/3$. Note that the relevant internal pion momentum is around 750 MeV. With all these approximations, we find

$$\Gamma(X_{b2} \to B\bar{B}) = \frac{3g^4 (g^{X_{b2}})^2}{5\pi f_\pi^4} \frac{m_B^2 m_{B^*}^4}{M_{X_{b2}}} |\vec{q}|^5 \left(I_0(m_{B^*}, m_\pi; M_{X_{b2}}, q^\mu[m_{F_1} = m_{F_2} = m_B]) \right)^2, \tag{29}$$

$$\Gamma(X_{b2} \to B\bar{B}^*) = \frac{9g^4 (g^{X_{b2}})^2}{10\pi f_\pi^4} \frac{m_B m_{B^*}^5}{M_{X_{b2}}} |\vec{q}|^5 \left(I_0(m_{B^*}, m_\pi; M_{X_{b2}}, q^\mu[m_{F_1} = m_B, m_{F_2} = m_{B^*}]) \right)^2, \tag{30}$$

for any charge channel (B^+B^-, $B^0\bar{B}^0$, B^+B^{*-}, $B^0\bar{B}^{*0}$) or charge conjugation mode ($B^*\bar{B}$). Our results for these decay widths are presented in Table III. We notice in passing that following heavy flavor symmetry we use the same value of $g = 0.570 \pm 0.006$ in the charm and bottom decays. It agrees very well with a recent lattice calculation with relativistic bottom quarks which gives $g_b = 0.569 \pm 0.076$ [47] (we have added the systematic and statistic errors in quadrature). Yet, lattice calculations with static heavy quarks tend to give smaller values, see Ref. [48] and references therein. For instance, the ALPHA Collaboration presented a precise computation with the result of $g_\infty = 0.492 \pm 0.029$ [48]. Thus we expect that the decay widths of Table III slightly overestimate the real ones.

For the $B\bar{B}$ mode we find a pronounced dependence on the Gaussian cutoff Λ employed in the dynamical generation of the resonance. This is inherited from the strong dependence of the X_{b2} mass on this UV cutoff, as discussed in Eq. (12), which affects the available phase space for the decay. With all these shortcomings, we expect a partial width in the 1-10 MeV range, when both charge modes are considered.

In the $B\bar{B}^*$ decay mode, the impact of the Gaussian regulator is even larger, because it turns out that for $\Lambda = 1$ GeV, the central value of the resonance mass $M_{X_{b2}} = 10594^{+22}_{-26}$ MeV is located below the threshold $m_B + m_{B^*} \sim 10604$ MeV. Thus, in that case, the decay will be forbidden. For $\Lambda = 0.5$ GeV, we estimate a width also in the 4-12 MeV range, when the four possible decay modes (B^+B^{*-}, $B^0\bar{B}^{*0}$, B^-B^{*+}, $\bar{B}^0B^{*0}$) are considered.

IV. THE X_2 AND X_{b2} RADIATIVE DECAYS

In this section, we will study the $X_2 \to D\bar{D}^*\gamma$ and $X_{b2} \to \bar{B}B^*\gamma$ decays. The interaction of the photon with the s-wave heavy mesons contains two contributions that correspond to the magnetic couplings to the light and heavy quarks [57] (see also Appendix A 3). Both terms are needed to understand the observed electromagnetic branching fractions of the D^{*+} and D^{*0} because a

	without pion-exchange FF		with pion-exchange FF	
	$\Lambda = 0.5$ GeV	$\Lambda = 1$ GeV	$\Lambda = 0.5$ GeV	$\Lambda = 1$ GeV
$\Gamma(X_{b2} \to B\bar{B})$ [MeV]	$26.0^{+1.0}_{-3.3}$	8^{+15}_{-7}	$4.4^{+0.1}_{-0.4}$	$0.7^{+1.4}_{-0.6}$
$\Gamma(X_{b2} \to B\bar{B}^*)$ [MeV]	$7.1^{+3.4}_{-3.7}$	–	$2.0^{+0.9}_{-1.0}$	–

TABLE III. $X_{b2} \to B\bar{B}, B\bar{B}^*$ decay widths (here $B\bar{B}^{(*)}$ refers to any of the neutral or charged modes, but it is not the sum of both). The results are given for different treatments of the three-point loop function. The errors have been obtained using the Monte Carlo analysis explained in Table I, but now considering the X_{b2} mass histograms displayed in Fig. 2 and the coupling given in Eq. (12). The decay width of the $X_{b2} \to \bar{B}B^*$ mode is the same because of charge conjugation symmetry.

cancellation between the two terms accounts for the very small width of the D^{*+} relative to the D^{*0} [5]. Actually, one finds [57, 58]:

$$\Gamma(D^{*0} \to D^0\gamma) = \frac{\alpha}{3}\frac{m_{D^0}}{m_{D^{*0}}}\left(\beta_1 + \frac{2}{3m_c}\right)^2 E_\gamma^3, \quad \beta_1 = \frac{2}{3}\beta - \frac{g^2 m_K}{8\pi f_K^2} - \frac{g^2 m_\pi}{8\pi f_\pi^2}, \tag{31}$$

$$\Gamma(D^{*+} \to D^+\gamma) = \frac{\alpha}{3}\frac{m_{D^+}}{m_{D^{*+}}}\left(\beta_2 + \frac{2}{3m_c}\right)^2 E_\gamma^3, \quad \beta_2 = -\frac{1}{3}\beta + \frac{g^2 m_\pi}{8\pi f_\pi^2}, \tag{32}$$

where E_γ is the photon energy, m_c the charm quark mass and $\alpha \sim 1/137.036$ the fine-structure constant. In the non-relativistic constituent quark model $\beta = 1/m_q \sim 1/330$ MeV^{-1}, where m_q is the light constituent quark mass. Heavy meson chiral perturbation theory allows one to improve upon this approximation by including corrections from loops with light Goldstone bosons, which give $\mathcal{O}(\sqrt{m_q})$ corrections [57].

Using isospin symmetry to relate $\Gamma(D^{*0} \to D^0\pi^0)$ and $\Gamma(D^{*+} \to D^0\pi^+)$, correcting by the slightly different available p-wave phase space in each of the two decays, and taking into account the experimental D^{*0} and D^{*+} widths and radiative branching fractions quoted by the PDG [5], we find:

$$\Gamma(D^{*0} \to D^0\gamma) = (22.7 \pm 2.6) \text{ keV}, \qquad \Gamma(D^{*+} \to D^+\gamma) = (1.33 \pm 0.33) \text{ keV}. \tag{33}$$

These values differ from those used in Ref. [58] because of the recent accurate BABAR measurement of the D^{*+} decay width, mentioned in Sect. III, which is around 10% smaller than the previous CLEO one used in Ref. [58]. Fixing the charm quark mass to $m_c = 1.5$ GeV, we fit the parameter β to the above experimental values and find $\beta^{-1} = (293 \pm 11)$ MeV.

In what follows, we will study decays of the type $X_2 \to P\bar{P}^*\gamma$, being P and P^* pseudoscalar and vector heavy-light mesons, respectively. Let us define p_1^μ, p_2^μ and p_3^μ as the four vectors of the final photon, pseudoscalar and vector mesons, respectively. Besides, let us define the invariant masses

$m_{ij}^2 = p_{ij}^2 = (p_i + p_j)^2$, which satisfy

$$m_{12}^2 + m_{13}^2 + m_{23}^2 = M_{X_2}^2 + m_1^2 + m_2^2 + m_3^2 = M_{X_2}^2 + m_P^2 + m_{P^*}^2. \tag{34}$$

Since, as we will see, the Feynman amplitudes depend only on the invariant masses m_{12}^2 and m_{23}^2 of the final γP and $P\bar{P}^*$ pairs, respectively, we can use the standard form for the Dalitz plot [5]

$$d\Gamma = \frac{1}{(2\pi)^3}\frac{1}{32M_{X_2}^3}\overline{|\mathcal{T}|}^2 dm_{23}^2 dm_{12}^2, \tag{35}$$

with $\overline{|\mathcal{T}|}^2$ the absolute value squared of the decay amplitude with the initial and final polarizations being averaged and summed, respectively. Thus, we readily obtain

$$\Gamma = \frac{1}{(2\pi)^3}\frac{1}{32M_{X_2}^3}\int_{(m_P+m_{P^*})^2}^{M_{X_2}^2} dm_{23}^2 \int_{(m_{12}^2)_{\rm min}}^{(m_{12}^2)_{\rm max}} dm_{12}^2 \overline{|\mathcal{T}|}^2, \tag{36}$$

where for a given value of m_{23}^2, the range of m_{12}^2 is determined by its values when $\vec{p}_P$ is parallel or anti-parallel to $\vec{p}_\gamma$ [5]:

$$\begin{aligned}(m_{12}^2)_{\rm max} &= (E_\gamma^* + E_P^*)^2 - (p_\gamma^* - p_P^*)^2,\\ (m_{12}^2)_{\rm min} &= (E_\gamma^* + E_P^*)^2 - (p_\gamma^* + p_P^*)^2,\end{aligned} \tag{37}$$

with $E_P^* = (m_{23}^2 + m_P^2 - m_{P^*}^2)/2m_{23}$ and $E_\gamma^* = (M_X^2 - m_{23}^2)/2m_{23}$ the energies of the P meson and photon in the m_{23} c.m. frame, respectively, and $p_{P,\gamma}^*$ the moduli of the corresponding 3-momenta.

Because of parity conservation, this is a p-wave decay and hence the photon momentum appears always in the amplitudes. In the X_2 rest frame, it is given by $|\vec{p}_\gamma| = E_\gamma = M_{X_2}^2 - m_{23}^2/(2M_{X_2})$.

A. $X_2(4013) \to D\bar{D}^*\gamma$

We will first consider the $X_2(4013) \to D^0\bar{D}^{*0}\gamma$ decay, which proceeds according to the Feynman diagrams depicted in Fig. 6. This decay can take place directly through the radiative transition of the constituent D^{*0} as shown in Fig. 6(a), which is the tree level approximation. However, there are other mechanisms driven by the $D\bar{D}^*$ FSI. After emitting the photon, the vector meson D^{*0} transits into the D^0, and it can interact with the other constituent in the X_2 as shown in Fig. 6(b). There is a third (c) mechanism in which the photon is emitted from the $\bar{D}^{*0}$ meson, and the virtual $D^{*0}\bar{D}^0$ rescatter into $D^0\bar{D}^{*0}$. Finally, Fig. 6(d) and (e) present another possibility, namely the decay can also occur through the charged $D^{*+}D^{*-}$ component of the X_2 resonance, and the virtual charged D^+D^{*-} and $D^{*+}D^-$ pairs then rescatter into $D^0\bar{D}^{*0}$. Because the X_2 has a well defined charge parity (+), the decay width into the charge conjugated mode $\bar{D}^0D^{*0}\gamma$ is the same. The Feynman diagrams contributing to the $D^+D^{*-}\gamma$ decay mode are similar with obvious replacements.

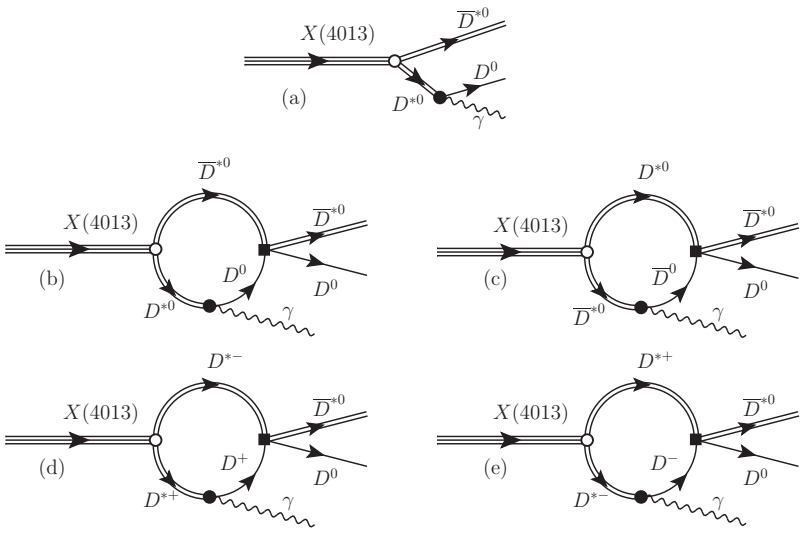

FIG. 6. Feynman diagrams for the $X_2(4013) \to D^0\bar{D}^{*0}\gamma$ decay. Diagrams for the $D^+D^{*-}\gamma$ transition are similar.

One could also construct other FSI mechanisms by replacing the $D^*D\gamma$ vertices in Fig. 6 with the $D^*D^*\gamma$ ones. These contributions are small and will be discussed below.

1. *Tree Level Approximation*

The Feynman amplitude of the mechanism depicted in Fig. 6(a) reads (as in the previous sections, we treat the charm mesons non-relativistically)

$$-i\mathcal{T}(\lambda,\lambda_*,\lambda_\gamma)_{D^0\bar{D}^{*0}\gamma} = g_0^{X_2}(m_{12})\sqrt{4\pi\alpha}N_\gamma\left(\beta_1+\frac{2}{3m_c}\right)\frac{\epsilon_{ijm}\epsilon^{jn}(\lambda)\epsilon^{*n}(\lambda_*)\epsilon_\gamma^{*i}(\lambda_\gamma)p_\gamma^m}{2m_{D^{*0}}\left(m_{12}-m_{D^{*0}}+i\varepsilon\right)}, \tag{38}$$

with m_{12} the invariant mass of the final γD^0 pair. Besides, $\epsilon^i(\lambda_\gamma)$ is the polarization vector of the final photon with helicity λ_γ, $\vec{p}_\gamma$ is its three momentum and $N_\gamma = \sqrt{8M_{X_2}m_{D^*}^2}\sqrt{m_D m_{D^*}}$ accounts for the normalization of the heavy meson fields and the $X_2D^{*0}\bar{D}^{*0}$ coupling. Finally,

$$g_0^{X_2}(m_{12}) = g_0^{X_2}\times e^{-(\vec{p}_{12}^2-\gamma^2)/\Lambda^2} = g_0^{X_2}\times e^{-m_{D^{*0}}(m_{D^{*0}}-m_{12})/\Lambda^2} \tag{39}$$

with $\vec{p}_{12}^2 \simeq m_{D^{*0}}(M_{X_2}-m_{D^{*0}}-m_{12})$ and $\gamma^2 = m_{D^{*0}}(M_{X_2}-2m_{D^{*0}}) < 0$. The Gaussian form factor is inherited from the $D^{(*)}\bar{D}^{(*)}$ EFT UV renormalization scheme.

We have neglected the D^{*0} width in the above propagator because, since it is quite small, its inclusion only leads to small numerical variations in the decay rate which are certainly smaller than uncertainties induced by the errors in the coupling $g_0^{X_2}$ and the mass of the $X_2(4013)$ resonance. Similarly, the use of the non-relativistic D^{*0} propagator instead of $\left(m_{12}^2-m_{D^{*0}}^2+i\varepsilon\right)^{-1}$ leads also

to numerically negligible differences, as compared to the HQSS corrections. The sum over the $\bar{D}^{*0}$, γ and X_2 polarizations can be easily done, and we get

$$\overline{|\mathcal{T}|}^2_{D^0\bar{D}^{*0}} = \frac{16\pi\alpha M_{X_2} m_{D^*} m_D}{3}\left(g_0^{X_2}(m_{12})\right)^2 \frac{\left(\beta_1+\frac{2}{3m_c}\right)^2}{\left(m_{12}-m_{D^{*0}}+i\varepsilon\right)^2}\vec{p}_\gamma^{\,2}. \tag{40}$$

The amplitude for $D^+\bar{D}^{*-}\gamma$ decay is readily obtained from Eq. (38) making the obvious replacements: $g_0^{X_2}\to g_c^{X_2}$, $\beta_1\to\beta_2$ and $(m_{D^0}, m_{D^{*0}})\to(m_{D^+}, m_{D^{*+}})$. Performing the phase space integration, we find at tree level (assuming the existence of the X_2 state)

$$\Gamma(X_2(4013)\to D^0\bar{D}^{*0}\gamma)_{\rm tree} = 18^{+2}_{-6}\left(16^{+2}_{-9}\right)\ \text{keV}, \tag{41}$$

$$\Gamma(X_2(4013)\to D^+D^{*-}\gamma)_{\rm tree} = 0.10^{+0.10}_{-0.05}\left(0.09^{+0.06}_{-0.03}\right)\ \text{keV}, \tag{42}$$

where the values outside and inside the parentheses are obtained with $\Lambda = 0.5$ and 1 GeV, respectively. The errors account for the uncertainty, both in the mass of the X_2 state and in its couplings $g_{0,c}^{X_2}$, derived from the $X(3872)$ input ($M_{X(3872)}$ and the ratio $R_{X(3872)}$ of the decay amplitudes for the $X(3872)\to J/\psi\rho$ and $X(3872)\to J/\psi\omega$ decays) and the HQSS corrections, as explained in the the caption of Table I. We have neglected additional uncertainties stemming from the error on β ($\simeq 3\%$), because it is totally uncorrelated to those discussed above, and it is much smaller than those affecting for instance the $g_{0,c}^{X_2}$ couplings. The neutral mode width is much larger than the charged one, thanks to the bigger magnetic $D^*D\gamma$ coupling and a larger available phase space.

In analogy with the discussion of Eqs. (20) and (21) in Ref. [33] for the $X(3872)\to D^0\bar{D}^0\pi^0$ decay, in the X_2 radiative processes the relative distance of the $D^*\bar{D}^*$ pair can be as large as allowed by the size of the $X_2(4013)$ resonance, since the final state is produced by the one body decay of the $\bar{D}^*$ meson instead of by a strong two body transition. Thus, the radiative $D\bar{D}^*\gamma$ decays might provide details on the long-distance part of the resonance wave function. For instance, the $d\Gamma/d|\vec{p}_{\bar{D}^{*0}}|$ [$d\Gamma/d|\vec{p}_{D^{*-}}|$] distribution is related to the $X_2(4013)$ wave-function $\Psi(\vec{p}_{\bar{D}^{*0}})$ [$\Psi(\vec{p}_{D^{*-}})$] [33]. This is in sharp contrast to the $D\bar{D}$ and $D\bar{D}^*$ decay modes studied in the previous sections, which turned out to be strongly sensitive to short distance dynamics of the resonance, as revealed by the notorious dependence on the UV form factors.

However, all these considerations are affected by the $D\bar{D}^*$ FSI effects to be discussed next.

2. $D\bar{D}^*$ FSI Effects

To account for the FSI effects, we include in the analysis the $D\bar{D}^*\to D\bar{D}^*$ and $D^*\bar{D}\to D\bar{D}^*$ T-matrices, which are obtained by solving the LSE [Eq. (A10)] in coupled channels with the $V_{D^{(*)}\bar{D}^{(*)}}$ potential given in Eq. (A8). Some isospin symmetry breaking effects are taken into account because

the physical masses of the neutral ($D\bar{D}^*$) and charged (D^+D^{*-}) channels are used in Eq. (A10). The $X_2 \to D^0\bar{D}^{*0}\gamma$ decay amplitude for the mechanisms depicted in Fig. 6(b) and (c) reads

$$-i\mathcal{T}(\lambda,\lambda_*,\lambda_\gamma)^{\rm FSI\,(b+c)}_{D^0\bar{D}^{*0}\gamma} = g_0^{X_2}\sqrt{4\pi\alpha}N_\gamma\left(\beta_1+\frac{2}{3m_c}\right)\epsilon_{ijm}\epsilon^{jn}(\lambda)\epsilon^{*n}(\lambda_*)\epsilon^{*i}_\gamma(\lambda_\gamma)p^m_\gamma \times 4m_D m_{D^*}\,\widehat{T}_{00\to00}(m_{23})\,J(m_{D^{*0}},m_{D^{*0}},m_{D^0},\vec{p}_\gamma)\ , \tag{43}$$

where m_{23} is the invariant mass of the final $D^0\bar{D}^{*0}$ pair,

$$\widehat{T}_{00\to00}(m_{23}) \equiv T_{D^0\bar{D}^{*0}\to D^0\bar{D}^{*0}}(m_{23}) + T_{D^{*0}\bar{D}^0\to D^0\bar{D}^{*0}}(m_{23}), \tag{44}$$

and the three-point loop integral function $J\,(M_1,M_2,M_3,\vec{p}_\gamma)$ is given in the Appendix C 2. The integral is convergent, however, for consistency it is evaluated using the same UV regularization scheme as that employed in the $D^{(*)}\bar{D}^{(*)}$ EFT. In sharp contrast with the hadronic decays studied above, the momenta involved in these integrals are rather low.

On the other hand, we see that in the (b)+(c) contribution there appears the combination $T_{D^0\bar{D}^{*0}\to D^0\bar{D}^{*0}}(m_{23})+T_{D^{*0}\bar{D}^0\to D^0\bar{D}^{*0}}(m_{23})$. In the isospin limit, when the mass differences between the neutral ($D^0\bar{D}^{*0}$) and charged (D^+D^{*-}) channels are neglected, we will find $\widehat{T}_{00\to00} = (T^{I=0}_{C=-1} + T^{I=1}_{C=-1})/2$. From Eqs. (A8) and (A10), we find the C-parity odd isospin amplitudes,[18]

$$\left[T^I_{C=-1}\right]^{-1}(m_{23}) = C^{-1}_{IZ} + G_{D\bar{D}^*}(m_{23}), \qquad I=0,1\ , \tag{45}$$

with $G_{D\bar{D}^*} \simeq G_{D^0\bar{D}^{*0}} \simeq G_{D^+\bar{D}^{*-}}$ a common loop function. Note that the kernel of this LSE is fixed by the isoscalar (C_{0Z}) and isovector (C_{1Z}) C(charge conjugation) $=-1$ terms of $V_{D^{(*)}\bar{D}^{(*)}}$. This is a trivial consequence of the conservation of this symmetry, taking into account that the X_2 and the photon are even and odd C-parity states, respectively.

The (d) and (e) FSI contributions of Fig. 6 are similar, with obvious replacements. We find

$$-i\mathcal{T}(\lambda,\lambda_*,\lambda_\gamma)^{\rm FSI\,(d+e)}_{D^0\bar{D}^{*0}\gamma} = g_c^{X_2}\sqrt{4\pi\alpha}N_\gamma\left(\beta_2+\frac{2}{3m_c}\right)\epsilon_{ijm}\epsilon^{jn}(\lambda)\epsilon^{*n}(\lambda_*)\epsilon^{*i}_\gamma(\lambda_\gamma)p^m_\gamma \times\left\{4m_D m_{D^*}\widehat{T}_{+-\to00}(m_{23})\right\}J(m_{D^{*+}},m_{D^{*+}},m_{D^+},\vec{p}_\gamma), \tag{46}$$

where

$$\widehat{T}_{+-\to00}(m_{23}) \equiv T_{D^+D^{*-}\to D^0\bar{D}^{*0}}(m_{23}) + T_{D^{*+}D^-\to D^0\bar{D}^{*0}}(m_{23}), \tag{47}$$

and in the isospin limit, we would have $\widehat{T}_{+-\to00} = (T^{I=0}_{C=-1} - T^{I=1}_{C=-1})/2$.

[18] Here and for simplicity we do not explicitly write the on-shell UV Gaussian form factors [see Eqs.(A10) and (A13)].

For the $X_2(4013) \to D^+ D^{*-}\gamma$ decay, the FSI contribution is

$$
\begin{aligned}
-i\mathcal{T}(\lambda,\lambda_*,\lambda_\gamma)^{\rm FSI}_{D^+\bar{D}^{*-}\gamma} &= \sqrt{4\pi\alpha}N_\gamma \epsilon_{ijm}\epsilon^{jn}(\lambda)\epsilon^{*n}(\lambda_*)\epsilon^{*i}_\gamma(\lambda_\gamma)p^m_\gamma \\
&\times 4m_D m_{D^*}\left\{ g_c^{X_2}\left(\beta_2+\frac{2}{3m_c}\right)\left[\widehat{T}_{+-\to+-}(m_{23})J(m_{D^{*+}},m_{D^{*+}},m_{D^+},\vec{p}_\gamma)\right]\right. \\
&\left. + g_0^{X_2}\left(\beta_1+\frac{2}{3m_c}\right)\left[\widehat{T}_{00\to+-}(m_{23})J(m_{D^{*0}},m_{D^{*0}},m_{D^0},\vec{p}_\gamma)\right]\right\}, \qquad (48)
\end{aligned}
$$

with

$$
\widehat{T}_{+-\to+-}(m_{23}) = T_{D^+D^{*-}\to D^+D^{*-}}(m_{23}) + T_{D^{*+}D^-\to D^+D^{*-}}(m_{23}), \qquad (49)
$$

$$
\widehat{T}_{00\to+-}(m_{23}) = T_{D^0\bar{D}^{*0}\to D^+D^{*-}}(m_{23}) + T_{D^{*0}\bar{D}^0\to D^+D^{*-}}(m_{23}) = \widehat{T}_{+-\to00}(m_{23}). \qquad (50)
$$

and $\widehat{T}_{+-\to+-}(m_{23}) = \widehat{T}_{00\to00}(m_{23})$ in the isospin limit.

Taking into account isospin corrections, induced by the meson mass differences, all the needed T-matrices ($\widehat{T}_{00\to00}, \widehat{T}_{+-\to00}$ and $\widehat{T}_{+-\to+-}$) can be calculated by solving the coupled channel LSE, Eq. (A10), with the $V_{D^{(*)}\bar{D}^{(*)}}$ potentials of Eq. (A8), as mentioned above. Thanks to the conservation of C-parity, the FSI corrections will depend only on C_{0Z} and C_{1Z}. Indeed, one finds

$$
\begin{pmatrix} \widehat{T}_{00\to00} & \widehat{T}_{+-\to00} \\ \widehat{T}_{00\to+-} & \widehat{T}_{+-\to+-} \end{pmatrix}^{-1} = \widehat{\mathcal{F}}_\Lambda^{-1}(E)\cdot\left\{ \begin{pmatrix} \frac{C_{0Z}+C_{1Z}}{2} & \frac{C_{0Z}-C_{1Z}}{2} \\ \frac{C_{0Z}-C_{1Z}}{2} & \frac{C_{0Z}+C_{1Z}}{2} \end{pmatrix}^{-1} - \begin{pmatrix} G_{D^0\bar{D}^{*0}} & 0 \\ 0 & G_{D^+\bar{D}^{*-}} \end{pmatrix} \right\}\cdot\widehat{\mathcal{F}}_\Lambda^{-1}(E)\,, \qquad (51)
$$

with $\widehat{\mathcal{F}}_\Lambda(E) = \mathrm{Diag}\left(f^{\rm neu}_\Lambda(E), f^{\rm ch}_\Lambda(E)\right)$, where the Gaussian form factors are defined after Eq. (A13).

The $Z_b(10610)$ observed in Ref. [59] carries electric charge, and its neutral partner was also reported by the Belle Collaboration [60]. It lies within a few MeV of the $B\bar{B}^*$ threshold and it is tempting to speculate about it as a hadronic molecule. Belle also reported the discovery of a second exotic electrically charged bottomonium state [59], $Z_b(10650)$ in the vicinity of the $B^*\bar{B}^*$ threshold. For both the $Z_b(10610)$ and $Z_b(10650)$ states, $J^P = 1^+$ are favored from angular analyses.

Within our scheme, we assume that the $Z_b(10610)$ resonance is an isovector $\left(B\bar{B}^* + B^*\bar{B}\right)/\sqrt{2}$ s-wave bound state with $J^{PC} = 1^{+-}$ [15]. Note, HQSS predicts the interaction of the $B^*\bar{B}^*$ system with $I = 1$, $J^{PC} = 1^+$ quantum numbers to be identical to that of the $B\bar{B}^*$ pair in the $Z_b(10610)$ sector. Thus, HQSS naturally explains [61] the approximate degeneracy of the $Z_b(10610)$ and $Z_b(10650)$. Taking for the $Z_b(10610)$ binding energy (2.0 ± 2.0) MeV [62], we could fix a third linear combination of the LECs that appear in the LO Lagrangian of Eq. (A6)

$$
C_{1Z} \equiv C_{1A} - C_{1B} = -0.75^{+0.10}_{-0.17}\ (-0.30^{+0.02}_{-0.04})\,\mathrm{fm}^2 \qquad (52)
$$

for $\Lambda = 0.5(1.0)$ GeV. Errors have been obtained with a procedure similar to that described in the discussion of Eq. (8) and used in the case of the $X(3872)$. Assuming heavy quark flavor symmetry,

the above value of C_{1Z} could be also used in the charm sector, subject to corrections of the order of $\mathcal{O}(\Lambda_{\rm QCD}/m_c) \simeq 20\%$ that we take into account. Therefore, we predict the existence of the isovector charmonium partners of the $Z_b(10610)$ and the $Z_b(10650)$, though as virtual states in the second Riemann sheet [15], which probably correspond to the recently observed charged charmonium-like[19] $Z_c(3900)$ and $Z_c(4025)$ states [63–67]. These resonances lie close to the $D\bar{D}^*$ and $D^*\bar{D}^*$ thresholds, respectively, while $J^P = 1^+$ quantum numbers are favored from some angular analyses.

Due to the presence of the $Z_c(3900)$ close to threshold, one should expect the loop (FSI) mechanisms depicted in Fig. 6 to be important since $T^{I=1}_{C=-1}$ must have a pole. However, the value of $C_{0Z} = (C_{0A} - C_{0B})$ is still unknown. It is not determined by the inputs deduced from the $X(3872)$ and $Z_b(10610)$ states used in the present analysis. Depending on the value of C_{0Z}, there can be an isoscalar $J^{PC} = 1^{+-}$ $D\bar{D}^*$ s-wave bound state or not. For instance, considering the case for $\Lambda = 0.5$ GeV and taking the central value for $C_{0Z} \sim -2.5$ fm^2 one finds a bound state pole in the $D\bar{D}^*$ system bound by around 10 MeV; if $C_{0Z} \sim -1.5$ fm^2, there will be a $D\bar{D}^*$ bound state almost at threshold; if the value of C_{0Z} is larger, there will be no bound state pole any more. Therefore, the information of C_{0Z} will be crucial in understanding the $D\bar{D}^*$ system and other exotic systems related to it through heavy quark symmetries [15, 35]. Conversely, as we will see, the X_2 radiative decay width could be used to extract information on the fourth LEC, C_{0Z}, thanks to the FSI effects.

To investigate the impact of the FSI, in Fig. 7 we show the dependence of the partial $X_2(4013) \to D\bar{D}^*\gamma$ decay widths on C_{0Z}. For comparison, the tree-level results are also shown in the same plots. As expected, for the decay into the $D^0\bar{D}^{*0}\gamma$ channel, the FSI effects turn out to be important, and for some values of C_{0Z}, they dominate the decay width. The maximum effects of the FSI mechanisms approximately occur for values of C_{0Z} which give rise to an isoscalar 1^{+-} $D\bar{D}^*$ bound or virtual state close to threshold. One can see an apparent deviation from the tree-level results in this region. When C_{0Z} takes smaller values, the binding energy of the bound state increases and moves apart from threshold; when C_{0Z} takes larger values, the pole moves deeper into a non-physical RS and becomes a virtual state further from the threshold. In both situations, the FSI corrections turn out to be less important. On the other hand, the FSI corrections are always important in the $D^+D^{*-}\gamma$ channel. This is because the tree level amplitude involves only the $D^{*\pm}D^{\pm}\gamma$ magnetic coupling, while FSI brings in the neutral magnetic coupling, which is much larger than the former one. This is also the reason, besides phase space, why the tree level width is much larger in the

[19] The simple EFT scheme employed in this work does not allow for finite width resonances, only for virtual or bound states. The merit of that EFT is actually making a connection between the $Z_b(10610/10650)$ and $Z_c(3900/4025)$ resonances on the basis of heavy flavor symmetry, not so much predicting the exact location. In that simple theory, we treat the $Z_b(10610)$ as a stable bound state and that is the reason why Z_c's are predicted to be virtual states. Had we used a more complete EFT that takes into account the finite width of the $Z_b(10610)$ and includes next-to-leading corrections, then we would have predicted the Z_c's as resonances and located them more accurately in the complex plane.

neutral mode than in the charged one, as commented above.

Notice that in the above calculations, we did not include the contribution from the coupled-channel FSI $D^*\bar{D}^* \to D\bar{D}^*$ which can come from replacing the $D^*D\gamma$ vertices in Fig. 6 by the $D^*D^*\gamma$ ones[20]. We have checked that this is a good approximation when the re-summation of the charmed meson scattering is switched off. This is partly because the loop integral defined in Eq. (C8) takes a much larger absolute value for the considered diagrams than for those with the $D^*D^*\gamma$ vertices in most regions of the phase space. The only exception is when the photon has a very low energy so that the $D^*\bar{D}^*$ are almost on-shell. However, after integrating over the phase space, this region provides a small contribution to the partial decay width because of the p_γ^3 suppression due to relative p-wave between the photon and the 1^{+-} $D\bar{D}^*$ system. The re-summation would introduce a further complication because of the presence of the $Z_c(4025)$ which couples dominantly to the $D^*\bar{D}^*$ in the 1^{+-} channel. It contributes mainly to the region close to the pole position of the $Z_c(4025)$. Again, this corresponds to the region with the very low-energy photon and thus it is suppressed due to phase space. Therefore, we expect that the neglected contribution discussed here has little impact, and its numerical effects should be safely covered by the sizable HQSS uncertainty exhibited in the results.

To better understand the dependence of the $X_2(4013) \to D\bar{D}^*\gamma$ decay widths on C_{0Z} in the bottom panel of Fig. 8 we show the pole positions of the odd C-parity $D\bar{D}^* \to D\bar{D}^*$ T-matrix as functions of this LEC and for an UV cutoff of 0.5 GeV. There are two coupled channels, the neutral one which has the lowest threshold, and the charged channel. As a consequence, there are three relevant RS's (among four). The first of them $[(++)]$ is the physical one, while the two non-physical RS's are reached by changing the sign of the imaginary part of the momentum inside of the loop functions G in Eq. (51) of the first channel $[(-+)]$ or the momenta of both channels $[(--)]$. Each of these non-physical RS's are continuously connected with the physical one on the real axis above the relevant thresholds. The solid red and dashed blue curves stand for poles in the $(++)$ and $(-+)$ RS's, respectively. For sufficiently large negative values of C_{0Z}, there is a bound state (a pole below threshold and located in the physical RS), which becomes less bound when $|C_{0Z}|$ decreases. For a value of this LEC around -1.5 fm^2, marked in Fig. 8 with a vertical black line, this state reaches the threshold. When C_{0Z} is further increased, the pole jumps into the $(-+)$ RS, becoming thus a virtual state (a pole below threshold and located in an non-physical RS) and it moves away from the threshold. In the medium panel we show the central values of the $X_2(4013)$ radiative widths for both decay modes as a function of C_{0Z}, which were already presented in Fig. 7. As can be seen, it

[20] The electric part of the $D^*D^*\gamma$ vertex does not contribute to the FSI X_2 decay width amplitude when the quantum numbers of the final $D^*\bar{D}^*$ pair are 1^{+-}, with the two heavy mesons in relative $s-$wave. Thus, we are left with the contribution from the magnetic coupling, as in the $D^*D\gamma$ case.

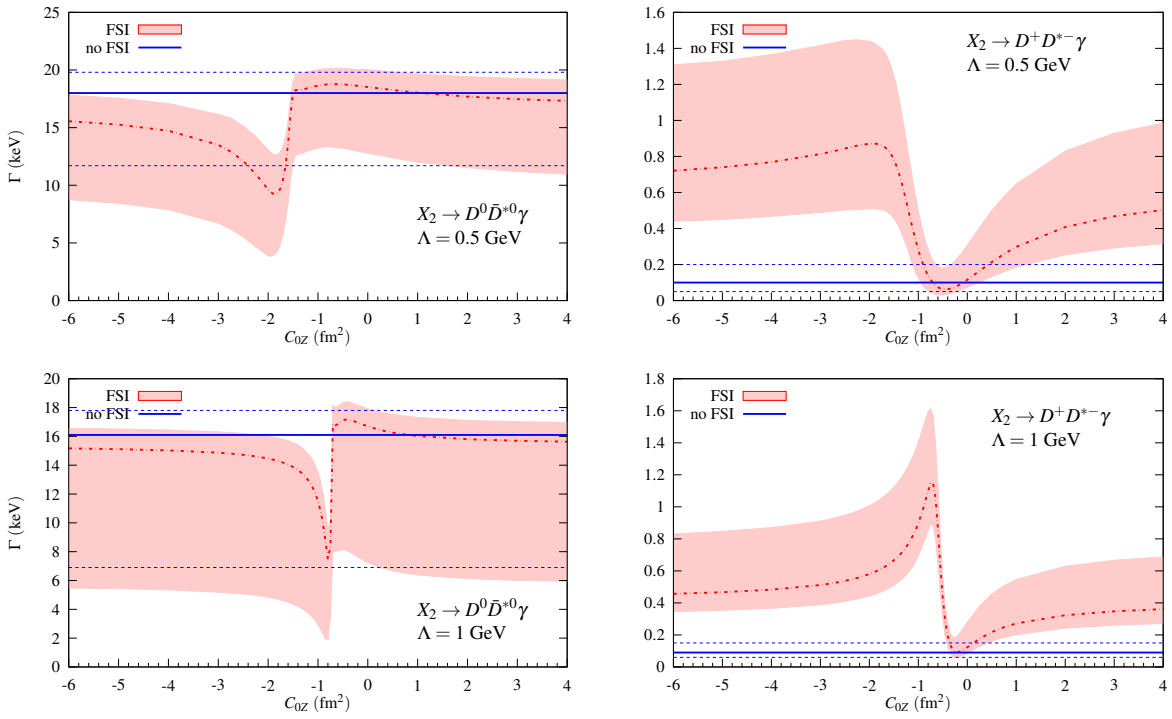

FIG. 7. Dependence of the $X_2(4013) \to D^0\bar{D}^{*0}\gamma$ and the $X_2(4013) \to D^+D^{*-}\gamma$ partial decay widths on the low-energy constant C_{0Z}. The UV cutoff is set to $\Lambda = 0.5$ GeV (1 GeV) in the top (bottom) panels. The red error bands contain the $D\bar{D}^*$ FSI effects, while the three horizontal blue lines stand for the tree level predictions of Eqs. (41) and (42). Besides the uncertainties on the mass and the couplings of the X_2 resonance, the errors on C_{1Z} quoted in Eq. (52), together with the expected 20% heavy quark flavor symmetry corrections when it is used in the charm sector, are also accounted in the 68% CL bands displayed in the panels. The red dash-dotted (full calculation) and solid blue (tree level) lines stand for the results obtained with the central values of the parameters.

is around this critical value $C_{0Z} = -1.5$ fm^2, when the FSI effects are larger for both decays, due to the vicinity of the pole to the threshold. This happens regardless of whether it is a bound or a virtual state, since the presence of the pole in both situations greatly enhances the odd C-parity $D\bar{D}^* \to D\bar{D}^*$ T-matrix near threshold. This can be appreciated in the top panel of Fig. 8, where the dependence of the $\widehat{T}_{00\to 00}$ and $\widehat{T}_{+-\to +-}$ scattering lengths on C_{0Z} is shown.

Thus we have understood why in the region of values of C_{0Z} around -1.5 fm^2, FSI corrections strongly affect the $D^0\bar{D}^{*0}\gamma$ decay width: this channel has the lowest threshold and the bound or virtual state is located on or nearby it. For the charged decay mode, the width exhibits a maximum for values of C_{0Z} also in this region, followed by a clear minimum placed now in the vicinity of $C_{0Z} \sim C_{1Z}$. Notice that when $C_{0Z} = C_{1Z}$, $\widehat{T}_{00\to +-}$ vanishes (see Eq. (51)) and therefore the contribution due to the neutral mesons, driven by the largest magnetic coupling (β_1), in the FSI loops disappears. The exact position of the minimum is modulated by the further interference

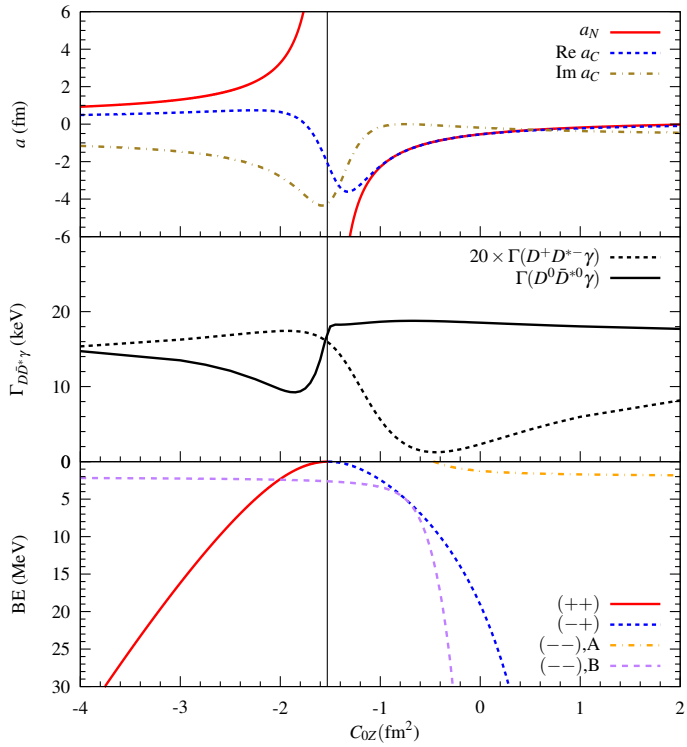

FIG. 8. Dependence on C_{0Z} of several physical quantities predicted in this work. In all cases an UV cutoff $\Lambda = 0.5$ GeV is employed in the Gaussian regulator. Top: $\widehat{T}_{00\to00}$ and $\widehat{T}_{+-\to+-}$ scattering lengths a_N (red solid curve) and a_C (blue dashed and green dash-dotted curves), respectively. They are defined as $a_i = \mu_i \widehat{T}_i(E = M_{1i} + M_{2i})/2\pi$, with μ_i the corresponding reduced mass and $(M_{1i}, M_{2i}) = (m_{D^0}, m_{D^{*0}})$ and $(m_{D^\pm}, m_{D^{*\pm}})$ for the neutral and charged channels, respectively. The scattering length a_C is complex because the neutral threshold is lower than the charged one, and therefore it is open. Middle: Central values of the $X_2(4013) \to D^0\bar{D}^{*0}\gamma$ (solid curve) and $X_2(4013) \to D^+D^{*-}\gamma$ (dashed curve) partial decay widths including FSI effects. Bottom: Position of the poles of the odd C-parity $D\bar{D}^* \to D\bar{D}^*$ T-matrix, with respect to the neutral $(m_{D^0} + m_{D^{*0}})$ threshold. Poles found in the various RS's are shown (see the text for details). The red solid curve shows the evolution of the bound state with C_{0Z}, while the dashed and the dash-dotted curves show that of the virtual ones. The vertical black line marks the value of C_{0Z} for which a $D\bar{D}^*$ bound state is generated at the $D^0\bar{D}^{*0}$ threshold.

between the tree level and the FSI charged loops, which are comparable.

In the bottom panel, we also observe a virtual state pole, the position of which is rather insensitive[21] to C_{0Z}. It is originated by the interaction in the $I = 1$ sector, C_{1Z}, and it should be related to

[21] The situation is more complicated, as can be seen in the plot. There is a narrow region of values of C_{0Z} around $[-0.4, -0.2]$ fm^2, where the virtual state moves quickly away from threshold, shortly reappearing again (orange dash-dotted line) in a position similar to the one that it had at the left of $C_{0Z} = -0.4$ fm^2. More in detail, in a narrow region included in the above interval of values of C_{0Z}, two poles (virtual) in the $(--)$ RS coexist. Among these two poles, the decay width should be influenced only by the one closest to threshold, since it overshadows the second one placed deeper in the real axis. On the other hand, for $C_{0Z} = -0.75$ fm^2 the $(--)$ RS virtual state (magenta, B) coincides with the one located in the $(-+)$ RS (blue). This is easy to understand since at this point $C_{0Z} = C_{1Z} \equiv C_Z$ and then according to Eq. (51) the off-diagonal interaction term vanishes. In this situation, neutral and charged channels decouple, the scattering length a_C is real, and the determinant $(1 - C_Z G_{D^0\bar{D}^{*0}})(1 - C_Z G_{D^+\bar{D}^{*-}})$ would

the $Z_c(3900)$ exotic charmonium-like state reported by the BESIII and Belle collaborations. Within our LO EFT scheme, we do not find a $D\bar{D}^*$ bound state, but instead a pole located near threshold in a non-physical RS [15].

vanish when either of the two factors in brackets is zero. It turns out that the factor $(1 - C_Z G_{D^0\bar{D}^{*0}})$ vanishes at the same energy both in the $(-+)$ and $(--)$ RS's, since by construction the $G_{D^0\bar{D}^{*0}}$ loop function is identical in both unphysical sheets. However, the charged factor $(1 - C_Z G_{D^+\bar{D}^{*-}})$ does not lead to any further pole for $C_{0Z} = C_{1Z} = -0.75$ fm^2 and $\Lambda = 0.5$ GeV. In the $\Lambda = 1$ GeV case, not shown in Fig. 8, it happens that for $C_{0Z} = C_{1Z} = -0.3$ fm^2, there exist identical poles in the $(-+)$ and $(--)$, and $(+-)$ and $(--)$ RS's, respectively, whose origin can be traced to the above discussion having in mind that now both terms in the decomposition of the determinant lead to poles.

B. $X_{b2} \to \bar{B} B^* \gamma$

The expressions found in the charm sector can be readily used here, having in mind the following correspondence: $D^0 \leftrightarrow B^-$, $D^+ \leftrightarrow \bar{B}^0$, $\bar{D}^0 \leftrightarrow \bar{B}^+$, and $D^- \leftrightarrow B^0$. Since the heavy quark flavor symmetry ensures that g and $\beta_{1,2}$ are the same in the b and c systems (up to corrections of the order $\Lambda_{\rm QCD}/m_c$), the expressions of Eqs. (31) and (32) can be used to predict the widths for the B^* radiative decays [57],

$$\Gamma(B^{*-} \to B^- \gamma) = \frac{\alpha}{3} \frac{m_B}{m_{B^*}} \left(\beta_1 - \frac{1}{3 m_b} \right)^2 E_\gamma^3 = (0.49 \pm 0.05) \text{ keV}, \tag{53}$$

$$\Gamma(\bar{B}^{*0} \to \bar{B}^0 \gamma) = \frac{\alpha}{3} \frac{m_B}{m_{B^*}} \left(\beta_2 - \frac{1}{3 m_b} \right)^2 E_\gamma^3 = (0.23 \pm 0.02) \text{ keV}, \tag{54}$$

where we have taken the value $m_b = 4.8$ GeV for the bottom quark mass.

As in the study of its hadronic decays, we assume the X_{b2} be a pure $I = 0$ state, with equal coupling to its neutral and charged components, $g_0^{X_{b2}} = g_c^{X_{b2}} = \frac{1}{\sqrt{2}} g^{X_{b2}}$. The isospin breaking effects for the B^* mesons are expected to be small and the tiny difference between the B^0 and $B^\pm$ masses can safely be neglected as well. In this limit we find at tree level

$$-i\mathcal{T}(\lambda, \lambda_*, \lambda_\gamma)_{\bar{B} B^* \gamma} = \frac{g^{X_{b2}}(m_{12})}{\sqrt{2}} \sqrt{4\pi\alpha} N_\gamma^b \left(\beta_a - \frac{1}{3 m_b} \right) \frac{\epsilon_{ijm} \epsilon^{jn}(\lambda) \epsilon^{*n}(\lambda_*) \epsilon_\gamma^{*i}(\lambda_\gamma) p_\gamma^m}{2 m_{B^*} \left(m_{12} - m_{B^*} + i\varepsilon \right)}, \tag{55}$$

where $\beta_a = \beta_1(\beta_2)$ for the $B^- B^{*+} \gamma (\bar{B}^0 B^{*0} \gamma)$ mode, $N_\gamma^b = \sqrt{8 M_{X_{b2}} m_{B^*}^2} \sqrt{m_B m_{B^*}}$, and m_{12} is the invariant mass of the final $\gamma \bar{B}$ pair. These amplitudes lead to

$$\Gamma(X_{b2} \to B^- B^{*+} \gamma)_{\rm tree} = 13^{+23}_{-10} \text{ eV}, \quad \Gamma(X_{b2} \to \bar{B}^0 B^{*0} \gamma)_{\rm tree} = 6^{+10}_{-5} \text{ eV}, \tag{56}$$

where the values have been obtained with $\Lambda = 0.5$ GeV. We remind that for $\Lambda = 1$ GeV, the central value of the resonance mass $M_{X_{b2}}$ is located below the threshold $(m_B + m_{B^*}) \sim 10604$ MeV and the decay is forbidden. The errors reflect the uncertainty in the inputs from the $X(3872)$ and the HQSS breaking corrections, as outlined in the caption of Table III; they are quite large and are dominated by those quoted for $g^{X_{b2}}$ in Eq. (12). The widths are of the order of a few eV, significantly smaller than those of the radiative decays of the B^{*0} and B^{*-} meson because of the quite reduced phase space available (~ 20 MeV) for this p-wave decay. They are also orders of magnitude smaller than $\Gamma(X_2 \to D^0 \bar{D}^{*0} \gamma)$ as a result of $\Gamma(D^{*0} \to D^0 \gamma) \gg \Gamma(B^* \to B \gamma)$.

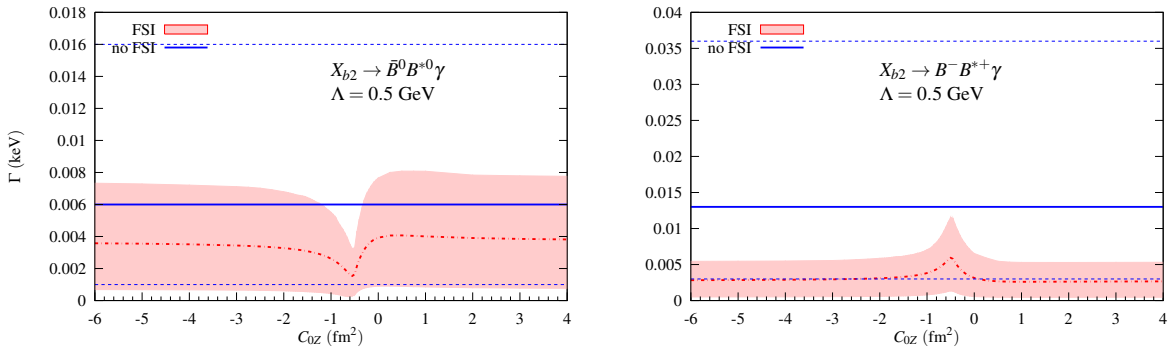

FIG. 9. Dependence of the $X_{b2} \to B^- B^{*+}\gamma$ and $X_{b2} \to \bar{B}^0 B^{*0}\gamma$ partial decay widths on the low-energy constant C_{0Z}. The red error bands contain the $\bar{B}B^*$ FSI effects, while the three horizontal blue lines stand for the tree level predictions of Eq. (56).

The amplitude for the FSI mechanisms is readily evaluated and we find

$$
\begin{aligned}
-i\mathcal{T}(\lambda,\lambda_*,\lambda_\gamma)^{\rm FSI}_{\bar{B}B^*\gamma} &= \sqrt{4\pi\alpha}N_\gamma^b \frac{g^{X_{b2}}}{\sqrt{2}}\epsilon_{ijm}\epsilon^{jn}(\lambda)\epsilon^{*n}(\lambda_*)\epsilon_\gamma^{*i}(\lambda_\gamma)p_\gamma^m J(m_{B^*},m_{B^*},m_B,\vec{p}_\gamma) \\
&\times 4m_B m_{B^*}\left\{\left(\beta_1-\frac{1}{3m_b}\right)\left[\frac{T^{I=0}_{C=-1}(m_{23})\pm T^{I=1}_{C=-1}(m_{23})}{2}\right]_{\bar{B}B^*}\right. \\
&\left.+\left(\beta_2-\frac{1}{3m_b}\right)\left[\frac{T^{I=0}_{C=-1}(m_{23})\mp T^{I=1}_{C=-1}(m_{23})}{2}\right]_{\bar{B}B^*}\right\},
\end{aligned}
\tag{57}
$$

where the $+-$ $(-+)$ combination stands for the $B^- B^{*+}\gamma$ ($\bar{B}^0 B^{*0}\gamma$) decay mode and m_{23} is now the invariant mass of the $\bar{B}B^*$ pair. The C-parity odd isospin amplitudes are obtained by solving Eq. (45) using the bottom sector loop function $G_{\bar{B}B^*}$.

FSI corrections turn out to be important, as can be appreciated in Fig. 9. This is because we are generating in the $T^{I=1}_{C=-1}$ amplitude a bound state [$Z_b(10610)$], almost at threshold (binding energy (2.0$\pm$2.0) MeV [62]), that enhances the loop mechanisms, as we discussed in the charm sector. If we pay attention for instance to the charged $B^- B^{*+}\gamma$ mode, we could appreciate a distinctive feature: there appears a destructive interference pattern between the tree level and the FSI amplitudes. Thanks to our MC procedure where correlations are consistently propagated, we also observe a reduction of the size in the uncertainties. Besides the uncertainties on the mass and the couplings of the X_{b2} resonance, the errors on C_{1Z} quoted in Eq. (52) are also accounted for in the 68% CL bands displayed in the panels. Actually, these latter uncertainties should have also an important impact on the total CL bands. This is because variations of C_{1Z} allow for situations where the pole is located precisely at threshold (zero binding energy) or bound by about 4 MeV. In the first case the FSI contribution should be larger than that obtained with the central value of C_{1Z}, which correspond to a binding energy of 2 MeV. These big 68% CL bands makes hard to disentangle any

further dependence on C_{0Z}, which in this case turns out to be quite mild.

V. CONCLUSIONS

In this work we have studied the hadronic and radiative decays of a molecular $P^*\bar{P}^*$ state with quantum numbers $J^{PC} = 2^{++}$ in the charm (X_2) and bottom (X_{b2}) sectors using an EFT approach. We have considered the $X(3872)$ resonance as a $J^{PC} = 1^{++}$ $D\bar{D}^*$ hadronic molecule. The X_2 and the X_{b2} states will be HQSFS partners of the $X(3872)$ with masses and couplings to the $P^*\bar{P}^*$ heavy meson pair determined by the properties of the $X(3872)$ resonance.

The hadronic d-wave $X_2 \to D\bar{D}$ and $X_2 \to D\bar{D}^*$ two-body decays are driven via one pion exchange. We observed that as a result of the contribution from highly virtual pions, which is out of control in the low-energy EFT, these hadronic decay widths (hence the total width of the X_2 as well) bear a large systematic uncertainty. Even though the momenta involved in these decays probably lie outside the range of applicability of EFT the calculations are still valuable as a way to find reasonable estimates of these partial decay widths, which we expect to almost saturate the X_2 decay width. To this end and in analogy to the Bonn potential, we have included a monopole pion-exchange form factor, with a cutoff around 1 GeV, in each of the $D^*D\pi$ and $D^*D^*\pi$ vertices to suppress the contribution of large momenta. We finally estimate the partial widths of both processes to be of the order of a few MeV. The analysis runs in parallel in the bottom sector with the assumption that the bare contact terms in the Lagrangian are independent of the heavy flavor. In this sector, we also find widths of the order of a few MeV.

We discussed the radiative $X_2 \to D\bar{D}^*\gamma$ and $X_{b2} \to \bar{B}B^*\gamma$ decays as well. The widths are small, of the order of keV's (eV's) in the charm (bottom) sectors. Furthermore, they are affected by the $D\bar{D}^*$ or $B\bar{B}^*$ FSI mechanisms. FSI effects are large because they are enhanced by the presence of the isovector $Z_c(3900)$ and $Z_b(10610)$ resonances located near the $D^0\bar{D}^{*0}$ and $\bar{B}B^*$ thresholds, respectively. In the charm sector, FSI corrections turn out to be also sensitive to the negative C-parity isoscalar $D\bar{D}^*$ interaction (C_{0Z}). Thus, future precise measurements of these radiative decay widths might provide valuable information on this LEC, which cannot be in principle determined from the properties of the $X(3872)$, $Z_b(10610)$ and $Z_b(10650)$ resonances. Constraints on this latter LEC are important in order to understand the dynamics of the $P^{(*)}\bar{P}^{(*)}$ system.

ACKNOWLEDGMENTS

We would like to thank C. Hanhart for discussions about the expected width of the X_2 that prompted us to initiate this work and for valuable comments. We are also very grateful to U. van Kolck for valuable discussions on the heavy flavor dependence of the contact terms. We thank U.-G. Meißner and E. Oset for careful proof readings and comments. C. H.-D. thanks the support of the JAE-CSIC Program and the hospitality of the HISKP during his visit. M. A. acknowledges financial support from the "Juan de la Cierva" program (reference 27-13-463B-731) from the Spanish Government through the Ministerio de Economía y Competitividad. This work is supported in part by the DFG and the NSFC through funds provided to the Sino-German CRC 110 "Symmetries and the Emergence of Structure in QCD" (NSFC Grant No. 11261130311), by the NSFC (Grant No. 11165005), by the Spanish Ministerio de Economía y Competitividad and European FEDER funds under the contract FIS2011-28853-C02-02 and the Spanish Consolider-Ingenio 2010 Programme CPAN (CSD2007-00042), by Generalitat Valenciana under contract PROMETEOII/2014/0068 and by the EU HadronPhysics3 project, grant agreement no. 283286.

Appendix A: Heavy meson Lagrangians: *s*-wave interactions and pionic and electromagnetic decays

We collect in this appendix the Lagrangians used in this work. We use the matrix field $H^{(Q)}$ $[H^{(\bar{Q})}]$ to describe the combined isospin doublet of pseudoscalar heavy-mesons $P_a^{(Q)} = (Q\bar{u}, Q\bar{d})$ $[P_a^{(\bar{Q})} = (u\bar{Q}, d\bar{Q})]$ fields and their vector HQSS partners $P_a^{*(Q)}$ $[P_a^{*(\bar{Q})}]$ (see for example [40]),

$$H_a^{(Q)} = \frac{1+\not{v}}{2}\left(P_{a\mu}^{*(Q)}\gamma^\mu - P_a^{(Q)}\gamma_5\right), \qquad v\cdot P_a^{*(Q)} = 0,$$
$$H_a^{(\bar{Q})} = \left(P_{a\mu}^{*(\bar{Q})}\gamma^\mu - P_a^{(\bar{Q})}\gamma_5\right)\frac{1-\not{v}}{2}, \qquad v\cdot P_a^{*(\bar{Q})} = 0. \tag{A1}$$

The matrix field H^c $[H^{\bar{c}}]$ annihilates P $[\bar{P}]$ and P^* $[\bar{P}^*]$ mesons with a definite velocity v. The field $H_a^{(Q)}$ $[H_a^{(\bar{Q})}]$ transforms as a $(2,\bar{2})$ $[(\bar{2},2)]$ under the heavy spin $\otimes$ SU(2)$_V$ isospin symmetry [40], this is to say:

$$H_a^{(Q)} \to S\left(H^{(Q)}U^\dagger\right)_a, \qquad H^{(\bar{Q})a} \to \left(UH^{(\bar{Q})}\right)^a S^\dagger. \tag{A2}$$

Their hermitian conjugate fields are defined by:

$$\bar{H}^{(Q)a} = \gamma^0 H_a^{(Q)\dagger}\gamma^0, \qquad \bar{H}_a^{(\bar{Q})} = \gamma^0 \bar{H}^{(\bar{Q})a\dagger}\gamma^0, \tag{A3}$$

and transform as [40]:

$$\bar{H}^{(Q)a} \to \left(U\bar{H}^{(Q)}\right)^a S^\dagger, \qquad \bar{H}_a^{(\bar{Q})} \to S\left(\bar{H}^{(\bar{Q})}U^\dagger\right)_a. \tag{A4}$$

The definition for $H_a^{(\bar{Q})}$ also specifies our convention for charge conjugation, which is $\mathcal{C}P_a^{(Q)}\mathcal{C}^{-1} = P^{(\bar{Q})a}$ and $\mathcal{C}P_{a\mu}^{*(Q)}\mathcal{C}^{-1} = -P_\mu^{*(\bar{Q})a}$, and thus it follows

$$\mathcal{C}H_a^{(Q)}\mathcal{C}^{-1} = c\,H^{(\bar{Q})aT}\,c^{-1}, \qquad \mathcal{C}\bar{H}^{(Q)a}\mathcal{C}^{-1} = c\,\bar{H}_a^{(\bar{Q})T}\,c^{-1} \tag{A5}$$

with c the Dirac space charge conjugation matrix satisfying $c\gamma_\mu c^{-1} = -\gamma_\mu^T$.

1. Quadruple-heavy-meson contact interaction

At very low energies, the interaction between a heavy and anti-heavy meson can be accurately described just in terms of a contact-range potential. The LO Lagrangian respecting HQSS reads [68]

$$\begin{aligned}\mathcal{L}_{4H} = {} & C_A\,\mathrm{Tr}\left[\bar{H}^{(Q)a}H_a^{(Q)}\gamma_\mu\right]\mathrm{Tr}\left[H^{(\bar{Q})a}\bar{H}_a^{(\bar{Q})}\gamma^\mu\right] \\ & + C_A^\tau\,\mathrm{Tr}\left[\bar{H}^{(Q)a}\vec{\tau}_a^{\,b}H_b^{(Q)}\gamma_\mu\right]\mathrm{Tr}\left[H^{(\bar{Q})c}\vec{\tau}_c^{\,d}\bar{H}_d^{(\bar{Q})}\gamma^\mu\right] \\ & + C_B\,\mathrm{Tr}\left[\bar{H}^{(Q)a}H_a^{(Q)}\gamma_\mu\gamma_5\right]\mathrm{Tr}\left[H^{(\bar{Q})a}\bar{H}_a^{(\bar{Q})}\gamma^\mu\gamma_5\right] \\ & + C_B^\tau\,\mathrm{Tr}\left[\bar{H}^{(Q)a}\vec{\tau}_a^{\,b}H_b^{(Q)}\gamma_\mu\gamma_5\right]\mathrm{Tr}\left[H^{(\bar{Q})c}\vec{\tau}_c^{\,d}\bar{H}_d^{(\bar{Q})}\gamma^\mu\gamma_5\right]\end{aligned} \tag{A6}$$

with $\vec{\tau}$ the Pauli matrices in isospin space, and $C_{A,B}^{(\tau)}$ light flavor independent LECs, which are also assumed to be heavy flavor independent. Note that in our normalization the heavy or anti-heavy meson fields, $H^{(Q)}$ or $H^{(\bar{Q})}$, have dimensions of $E^{3/2}$ (see [69] for details). This is because we use a non-relativistic normalization for the heavy mesons, which differs from the traditional relativistic one by a factor $\sqrt{M_H}$. For later use, the four LECs that appear above are rewritten into C_{0A}, C_{0B} and C_{1A}, C_{1B} which stand for the LECs in the isospin $I = 0$ and $I = 1$ channels, respectively. The relations read

$$C_{0\phi} = C_\phi + 3C_\phi^\tau, \qquad C_{1\phi} = C_\phi - C_\phi^\tau, \qquad \text{for } \phi = A, B\ . \tag{A7}$$

The LO Lagrangian determines the contact interaction potential $V = -\mathcal{L}/4$, which is then used as kernel of the two body elastic LSE (see Eq. (4) and the related discussion).

The LECs that appear in the $J^{PC} = 1^{++}$ and 2^{++} sectors [Eqs. (3) and (9)] turn out to be $C_{0X} \equiv C_{0A} + C_{0B}$ and $C_{1X} \equiv C_{1A} + C_{1B}$. The contact interaction in the $Z_b(10610)$ sector ($I = 1$, $J^{PC} = 1^{+-}$) is $C_{1Z} \equiv C_{1A} - C_{1B}$.

On the other hand, the interaction in the $\{D^0\bar{D}^{*0}, D^{*0}\bar{D}^0, D^+D^{*-}, D^{*+}D^-\}$ space reads:[22]

$$V_{D^{(*)}\bar{D}^{(*)}} = A^T \times \text{Diag}(C_{0Z}, C_{0X}, C_{1Z}, C_{1X}) \times A$$
$$= \frac{1}{2}\begin{pmatrix} C_{0A}+C_{1A} & -C_{0B}-C_{1B} & C_{0A}-C_{1A} & C_{1B}-C_{0B} \\ -C_{0B}-C_{1B} & C_{0A}+C_{1A} & C_{1B}-C_{0B} & C_{0A}-C_{1A} \\ C_{0A}-C_{1A} & C_{1B}-C_{0B} & C_{0A}+C_{1A} & -C_{0B}-C_{1B} \\ C_{1B}-C_{0B} & C_{0A}-C_{1A} & -C_{0B}-C_{1B} & C_{0A}+C_{1A} \end{pmatrix}, \tag{A8}$$

with $C_{0Z} = C_{0A} - C_{0B}$ and the orthogonal matrix A given by:

$$A = \frac{1}{2}\begin{pmatrix} 1 & 1 & 1 & 1 \\ 1 & -1 & 1 & -1 \\ 1 & 1 & -1 & -1 \\ 1 & -1 & -1 & 1 \end{pmatrix}. \tag{A9}$$

Equation (A8) trivially follows from the fact that the $\mathcal{L}_{4H}$ interaction of Eq. (A6) is diagonal in the isospin basis and the charge conjugation is well defined.[23] The interaction given in Eq. (A8) can be used as the kernel of an UV finite LSE to obtain the T-matrix that we use to account for the FSI in the radiative decays studied in Section IV,

$$[T_{D^{(*)}\bar{D}^{(*)}}(E)]^{-1} = \mathcal{F}_\Lambda^{-1}(E) \cdot \left\{[V_{D^{(*)}\bar{D}^{(*)}}]^{-1} - \widehat{G}(E)\right\} \cdot \mathcal{F}_\Lambda^{-1}(E), \tag{A10}$$

with the two particle regularized matrix propagator defined as

$$\widehat{G}(E) = \text{Diag}\left(G_{D^0\bar{D}^{*0}}, G_{D^{*0}\bar{D}^0}, G_{D^+D^{*-}}, G_{D^{*+}D^-}\right), \tag{A11}$$

$$G_{ij}(E) = \int \frac{d^3\vec{q}}{(2\pi)^3} \frac{e^{-2\vec{q}^2/\Lambda^2}}{E - \vec{q}^2/2\mu_{ij} - M_i - M_j + i\varepsilon}, \tag{A12}$$

where trivially $G_{D^0\bar{D}^{*0}} = G_{D^{*0}\bar{D}^0}$ and $G_{D^+D^{*-}} = G_{D^{*+}D^-}$. In addition, the on-shell UV Gaussian form factor matrix reads

$$\mathcal{F}_\Lambda(E) = \text{Diag}\left(f_\Lambda^{\text{neu}}(E), f_\Lambda^{\text{neu}}(E), f_\Lambda^{\text{ch}}(E), f_\Lambda^{\text{ch}}(E)\right) \tag{A13}$$

with $f_\Lambda^{(a)}(E) = \exp(-\vec{k}_a^2/\Lambda^2)$ and $\vec{k}_a^2 = 2\mu_a(E - M_{1a} - M_{2a})$, with $a = (\text{neu}), (\text{ch})$.

2. $P^{(*)}\bar{P}^{(*)}\pi$ interactions

The relevant term in the LO Lagrangian of the heavy meson chiral perturbation theory [40–43] that provides the $D^*D\pi$ and $D^*D^*\pi$ couplings is

$$\mathcal{L}_{\pi HH} = -\frac{g}{2f_\pi}\left(\text{Tr}\left[\bar{H}^{(Q)b}H_a^{(Q)}\gamma_\mu\gamma_5\right] + \text{Tr}\left[H^{(\bar{Q})b}\bar{H}_a^{(\bar{Q})}\gamma^\mu\gamma_5\right]\right)(\vec{\tau}\partial_\mu\vec{\phi})_b^a + \cdots, \tag{A14}$$

[22] In the bottom sector, the corresponding basis is: $\{B^-B^{*+}, B^{*-}B^+, \bar{B}^0B^{*0}, \bar{B}^{*0}B^0\}$.

[23] For instance in the charm sector, the C-parity states are $[D\bar{D}^*]_{1,2} = \frac{D\bar{D}^* \pm D^*\bar{D}}{\sqrt{2}}$ $(1 \leftrightarrow +, 2 \leftrightarrow -)$. In our convention, the C-parity of these states is independent of the isospin and it is equal to ∓ 1.

with $\vec{\phi}$ a relativistic field that describes the pion,[24] g is the heavy flavor independent $PP^*\pi$ coupling and $f_\pi = 92.2\,\text{MeV}$ the pion decay constant. Note that in our normalization, the pion field has a dimension of energy, while the heavy meson or antimeson fields $H^{(Q)}$ or $H^{(\bar{Q})}$ have dimensions of $E^{3/2}$, as we already mentioned.

3. $HH\gamma$ interactions

The magnetic coupling of the photon to the s-wave heavy mesons is described by the Lagrangian [57, 58]

$$\begin{aligned}\mathcal{L}_{\gamma HH} = &\frac{e\beta}{4}Q_b^a\left(\text{Tr}\left[\bar{H}^{(Q)b}H_a^{(Q)}\sigma^{\mu\nu}\right] + \text{Tr}\left[H^{(\bar{Q})b}\bar{H}_a^{(\bar{Q})}\sigma^{\mu\nu}\right]\right)F_{\mu\nu}\\ &+\frac{eQ'}{4m_Q}\left(\text{Tr}\left[\bar{H}^{(Q)a}\sigma^{\mu\nu}H_a^{(Q)}\right] + \text{Tr}\left[H^{(\bar{Q})a}\sigma^{\mu\nu}\bar{H}_a^{(\bar{Q})}\right]\right)F_{\mu\nu} + \cdots\end{aligned} \tag{A15}$$

where $F_{\mu\nu} = \partial_\mu A_\nu - \partial_\nu A_\mu$, with A_μ the photon field ($\mathcal{C}A_\mu(x)\mathcal{C}^{-1} = -A_\mu(x)$), $Q = \text{Diag}(2/3, -1/3)$ is the light quark charge matrix, and Q' is the heavy quark electric charge (in units of the proton charge $e = \sqrt{4\pi\alpha}$). For charm (bottom) $Q' = 2/3$ ($Q' = -1/3$). Besides, m_Q is the heavy quark mass and β is the parameter introduced in Ref. [57]. These two terms describe the magnetic coupling due to the light (preserves HQSS) and heavy quarks (suppressed by $1/m_Q$), respectively. Both terms are needed to understand the observed electromagnetic branching fractions of the D^{*+} and D^{*0} because a cancellation between the two terms accounts for the very small width of the D^{*+} relative to the D^{*0} [5].

In the non-relativistic constituent quark model $\beta = 1/m_q \sim 1/330\ \text{MeV}^{-1}$, where m_q is the light constituent quark mass. Heavy meson chiral perturbation theory provides contributions from Goldstone boson loops, which give $\mathcal{O}(\sqrt{m_q})$ corrections to the decay rates [57]. If these loop corrections are evaluated in an approximation where heavy hadron mass differences are neglected, the correction to the above formulas can be incorporated by making the following replacements [57]

$$\beta Q_{11} \to \beta Q_{11} - \frac{g^2 m_K}{8\pi f_K^2} - \frac{g^2 m_\pi}{8\pi f_\pi^2}, \tag{A16}$$

$$\beta Q_{22} \to \beta Q_{22} + \frac{g^2 m_\pi}{8\pi f_\pi^2}, \tag{A17}$$

with $f_K \sim 1.2 f_\pi$.

[24] We use a convention such that $\phi = \frac{\phi_x - \mathrm{i}\phi_y}{\sqrt{2}}$ creates a π^- from the vacuum or annihilates a π^+, and the ϕ_z field creates or annihilates a π^0. We adopt the usual convention $\mathcal{C}(\vec{\tau}\cdot\vec{\phi})\mathcal{C}^{-1} = (\vec{\tau}\cdot\vec{\phi})^T$.

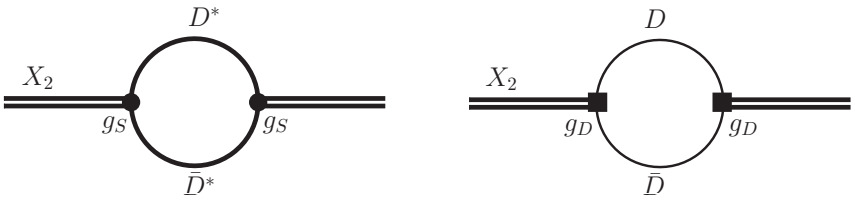

FIG. 10. The X_2 self-energy diagrams from the s-wave $D^*\bar{D}^*$ and d-wave $D\bar{D}$, respectively.

Appendix B: Validity of the perturbative treatment of the $D\bar{D}$ for the X_2

In this appendix, we will argue that the d-wave $D\bar{D}$ may be treated perturbatively in the 2^{++} system. Even though this was already discussed in Ref. [7], we have included here a new argument grounded on a different EFT to make a more compelling case on the smallness of this contribution to the X_2 mass. We will compare the power counting of the self-energy diagrams of the X_2 from the d-wave $D\bar{D}$ and the s-wave $D^*\bar{D}^*$ two-point loops, see Fig. 10. If the $D\bar{D}$ loop is suppressed in comparison with the $D^*\bar{D}^*$ one, it will validate the perturbative treatment of the $D\bar{D}$. Because in our case the heavy mesons are non-relativistic, we can apply a velocity counting for the loops analogous to the power counting of the heavy meson loops in heavy quarkonium transitions [70, 71].

For the $D^*\bar{D}^*$ loop, the velocity counting of the self-energy reads as

$$\Sigma_{D^*\bar{D}^*} \sim g_S^2 \frac{v^5}{(v^2)^2} = g_S^2\, v, \tag{B1}$$

where g_S denotes the value of the s-wave coupling of the X_2 to the $D^*\bar{D}^*$, v denotes the velocity of the D^* meson, v^5 is for the loop integral measure since the non-relativistic energy is counted as $\mathcal{O}(v^2)$, and $1/(v^2)^2$ accounts for the two non-relativistic propagators.

Similarly, for the $D\bar{D}$ loop, denoting the velocity of the D meson by w, the velocity counting is given by

$$\Sigma_{D\bar{D}} \sim g_D^2 \frac{w^5 w^4}{(w^2)^2} = g_D^2\, w^5, \tag{B2}$$

where g_D is the d-wave coupling constant normalized to have the same dimension as g_S, and the factor of w^4 in the denominator comes from the two d-wave vertices.

Therefore, we obtain the ratio

$$r_{D/S} \equiv \frac{\Sigma_{D\bar{D}}}{\Sigma_{D^*\bar{D}^*}} = \frac{g_D^2}{g_S^2}\frac{w^5}{v}. \tag{B3}$$

The question is now how g_D compares with g_S. We can estimate g_D by considering the one-pion exchange diagram considered in this work as illustrated in Fig. 11. Because the X_2 is very close to

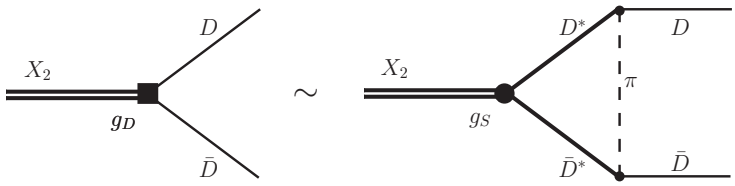

FIG. 11. The contact term of the d-wave coupling of the X_2 to the $D\bar{D}$ may be estimated by the one-pion exchange diagram.

the $D^*\bar{D}^*$ threshold, we should count each of the $D^*(\bar{D}^*)$ propagators as $1/v^2$. This is equivalent to affirm that the cut due to the $D^*\bar{D}^*$ in the triangle diagram in Fig. 11 is the same as that in the $D^*\bar{D}^*$ bubble diagram of the X_2 self-energy. Thus, we can count the D^* in both diagrams in the same way. But the pion propagator should be counted differently. The reason is that because the X_2 couples to the $D\bar{D}$ in a d-wave, the momenta in the $D^*D\pi$ vertices of the one-pion exchange diagram should become the momenta of the D and $\bar{D}$, $q_D = m_D w$, and the pion momentum is of the same order as we discussed in Sect. III A 1. This is to say that the pion propagator should be counted as $1/w^2$ rather than $1/v^2$. Thus, expressing the content of Fig. 11 in terms of power counting gives

$$g_D w^2 \sim g_S \frac{v^5}{(v^2)^2 w^2} \left(\frac{g}{\Lambda_\chi}\right)^2 (m_D w)^2 = \left[g_S g^2 \frac{v}{w^2} \left(\frac{m_D}{\Lambda_\chi}\right)^2\right] w^2, \tag{B4}$$

where g is the axial coupling constant in Eq. (A14), and $\Lambda_\chi = 4\pi f_\pi$ is the hard scale for the chiral expansion.

Numerically, for the case of the X_2, we have $w \simeq \sqrt{(M_{X_2} - 2m_D)/m_D} \simeq 0.38$, and $v \simeq \sqrt{(M_{X_2} - 2m_{D^*})/m_{D^*}} \sim 0.06$ if we take 7 MeV as the binding energy (recall that we have the charged $D^*\bar{D}^*$ channel explicitly whose threshold is around 7 MeV above the neutral one). With these values, we use Eqs. (B3) and (B4), which leads to $g_D \sim 0.6\, g_S$, to obtain an estimate of the contribution of the d-wave $D\bar{D}$ to the X_2 self-energy relative to the s-wave $D^*\bar{D}^*$,

$$r_{D/S} \sim 0.05. \tag{B5}$$

The above value suggests a high suppression of the d-wave $D\bar{D}$ in comparison with the s-wave $D^*\bar{D}^*$. We notice that the power counting of Ref. [7] indicates that the size of the $D\bar{D}$ loop is N^{4}LO (next-to-next-to-next-to-next-to-leading order), in line with the velocity power counting arguments.

Appendix C: Three-point loop functions

1. Hadron decays

In this section we address the tensor three-point loop function that appears in the hadron decay amplitudes studied in the Sect. III. It is composed by a pion, and two heavy meson ($P^*\bar{P}^*$) propagators. The integral reads ($\vec{q}=-\vec{k}$, $q^0+k^0=M_{X_2}$)

$$I^{ij}(M,m;M_{X_2},q^\mu) = i\int \frac{d^4l}{(2\pi)^4}\frac{l^i\,l^j}{[(l+q)^2-M^2+i\varepsilon]\,[(k-l)^2-M^2+i\varepsilon]\,(l^2-m^2+i\varepsilon)}$$
$$\simeq \frac{i}{4M^2}\int \frac{d^4l}{(2\pi)^4}\frac{l^i\,l^j}{(l^0+q^0-\omega_h+i\varepsilon)\,(k^0-l^0-\omega_h+i\varepsilon)\,(l^2-m^2+i\varepsilon)}, \quad \text{(C1)}$$

where M is the mass of the heavy particles in the loop, m is the mass for the light intermediate particle, M_{X_2} is the total c.m. energy, and q and k are the external 4-momenta of the two particles in the final state of masses m_{F_1} and m_{F_2}, respectively. In addition,

$$q^0=\frac{M_{X_2}^2+m_{F_1}^2-m_{F_2}^2}{2M_{X_2}}, \quad k^0=\frac{M_{X_2}^2+m_{F_2}^2-m_{F_1}^2}{2M_{X_2}}, \quad \text{(C2)}$$

and $\omega_h = M+(\vec{q}+\vec{l}\,)^2/2M$ is the non-relativistic energy of the virtual heavy mesons. Using Cauchy's theorem to integrate over the virtual pion energy l^0, we obtain:[25]

$$I^{ij}(M,m;M_{X_2},q^\mu)\simeq\frac{1}{4M^2}\int\frac{d^3l}{(2\pi)^3}l^il^j\frac{M_{X_2}-2\omega_h-2\omega}{2\omega(k^0-\omega-\omega_h)(q^0-\omega-\omega_h)(M_{X_2}-2\omega_h)}\,, \quad \text{(C3)}$$

for $|m_{F_1}^2-m_{F_2}^2|<2mM_{X_2}<4Mm$ to guarantee that the integral in Eq. (C1) is real, and $\omega(\vec{l}\,)=\sqrt{m^2+\vec{l}^{\,2}}$. The loop integral I^{ij} presents a logarithmic UV divergence. Indeed, I^{ij} admits a tensor decomposition

$$I^{ij}(\vec{q})=I_0(\vec{q}^{\,2})\,q^iq^j+I_1(\vec{q}^{\,2})\,\delta^{ij}\,|\vec{q}\,|^2\,. \quad \text{(C4)}$$

The I_1 term presents an UV divergence, but it does not contribute to the amplitude because it annihilates the traceless spin-2 polarization tensor. This means that only the I_0 term is relevant. It can be computed as:

$$I_0(M,m;M_{X_2},\vec{q}^{\,2})$$
$$\simeq\frac{1}{32M^2\pi^2\vec{q}^{\,2}}\int_0^{+\infty}\frac{dl\,l^4}{\omega}\int_{-1}^{+1}dxP_2(x)\frac{M_{X_2}-2\omega_h(l,x)-2\omega}{(k^0-\omega-\omega_h(l,x))(q^0-\omega-\omega_h(l,x))(M_{X_2}-2\omega_h(l,x))}, \quad \text{(C5)}$$

with $\omega_h(l,x)=M+(\vec{l}^{\,2}+\vec{q}^{\,2}+2|\vec{l}\,||\vec{q}\,|x)/2M$, and P_2 the Legendre's polynomial of order 2. This term is not UV divergent because in the limit $l\to+\infty$ all dependence on x, besides $P_2(x)$, disappears and

[25] If $m_{F_1}=m_{F_2}$, $k^0=q^0=M_{X_2}/2$ and the loop function now reads,

$$I^{ij}(M,m;M_{X_2},\vec{q}\,)\simeq\frac{1}{8M^2}\int\frac{d^3l}{(2\pi)^3}\frac{l^il^j}{\omega(M_{X_2}/2-\omega-\omega_h)(M_{X_2}/2-\omega_h)}, \quad M_{X_2}<2M\,.$$

the integration over x gives zero. The convergence of the integral is greatly enhanced because $P_2(x)$ is orthogonal to x as well. Moreover, the same type of arguments guarantees that $I_0(M,m;M_{X_2},\vec{q}^{\,2}) \sim$ const. in the $\vec{q}^{\,2} \to 0$ limit. Numerically, we use non-relativistic kinematics to compute $|\vec{q}|$ in the evaluation of $I_0(M,m;M_{X_2},\vec{q}^{\,2})$ in Eq. (C5), *i.e.*, $\vec{q}^{\,2} \simeq 2\mu_{F_1F_2}(M_{X_2}-m_{F_1}-m_{F_2})$. However, to guarantee the appropriate d-wave phase space, we use relativistic kinematics to evaluate q^iq^j in Eq. (C4) and the $|\vec{q}|$ phase-space factor that appears in Eqs. (15) and (21).

For consistency with the scheme adopted in Eq. (5), we include a Gaussian regulator in the $P^*\bar{P}^*X_2$ vertex by multiplying the integrand in Eq. (C5) by the exponential factor,

$$\frac{e^{-\left(\vec{q}+\vec{l}\right)^2/\Lambda^2}}{e^{-\gamma^2/\Lambda^2}} = \frac{e^{-\left(\vec{l}^{\,2}+\vec{q}^{\,2}+2|\vec{l}||\vec{q}|x\right)/\Lambda^2}}{e^{-\gamma^2/\Lambda^2}} \tag{C6}$$

with $0 > \gamma^2 = M(M_{X_2}-2M)$. We divide by the factor $e^{-\gamma^2/\Lambda^2}$, because it was incorporated in the $P^*\bar{P}^*X_2$ coupling.

In addition, the exchanged pion is highly virtual, and one might include a vertex form factor of the form

$$F(\vec{l}^{\,2},\Lambda_\pi) = \frac{\Lambda_\pi^2}{\vec{l}^{\,2}+\Lambda_\pi^2}, \qquad \Lambda_\pi \sim 1 \text{ GeV}, \tag{C7}$$

in each of the two $\pi P^{(*)}P^{(*)}$ vertices.

2. Radiative decays

In the computation of the FSI effects on the radiative decays of the X_2 and X_{b2} resonances in the Sect. IV, the following three-point loop function appeared

$$\begin{aligned} J\left(M_1,M_2,M_3,\vec{p}_\gamma\right) &= i\int \frac{d^4q}{(2\pi)^4}\frac{1}{q^2-M_1^2+i\varepsilon}\frac{1}{(P-q)^2-M_2^2+i\varepsilon}\frac{1}{(q-p_\gamma)^2-M_3^2+i\varepsilon} \qquad \text{(C8)}\\ &\simeq \frac{i}{8M_1M_2M_3}\int\frac{d^4q}{(2\pi)^4}\frac{1}{q^0-M_1-\vec{q}^{\,2}/2M_1+i\varepsilon}\frac{1}{M_{X_2}-q^0-M_2-\vec{q}^{\,2}/2M_2+i\varepsilon}\\ &\times\frac{1}{q^0-E_\gamma-M_3-(\vec{q}-\vec{p}_\gamma)^2/2M_3+i\varepsilon}\\ &= \frac{\mu_{12}\mu_{23}}{2M_1M_2M_3}\int\frac{d^3q}{(2\pi)^3}\frac{1}{(\vec{q}^{\,2}+c-i\varepsilon)}\frac{1}{(\vec{q}^{\,2}-2\mu_{23}\,\vec{q}\cdot\vec{p}_\gamma/M_3+c'-i\varepsilon)}, \qquad \text{(C9)} \end{aligned}$$

with $P^\mu = (M_{X_2},\vec{0})$ in the rest frame of the X_2 and $\mu_{ij}^{-1} = (M_i^{-1}+M_j^{-1})$. In addition, $b_{12} = M_1+M_2-M_{X_2}$, $b_{23} = M_2+M_3+E_\gamma-M_{X_2}$, $c = 2\mu_{12}b_{12}$ and $c' = 2\mu_{23}b_{23}+\mu_{23}\vec{p}_\gamma^{\,2}/M_3$. Since all the intermediate mesons in the present case are non-relativistic, the three point loop has been treated non-relativistically. This loop integral is convergent and its analytic expression can be found in Eq. (A2) of Ref. [71]. However, for consistency, despite the three-point loop function in Eq. (C8)

being finite, it should be evaluated using the same UV renormalization scheme as that employed in the $D^{(*)}\bar{D}^{(*)}$ EFT. This is accomplished by including in the integrand of Eq. (C8) a Gaussian form factor, $F_\Lambda(\vec{q})$ defined as

$$F_\Lambda(\vec{q}) = e^{-(\vec{q}^2-\gamma^2)/\Lambda^2} e^{-(\vec{q}^2_{\rm cm}-\vec{q}^2_{\rm on\,shell})/\Lambda^2}. \tag{C10}$$

Here $\gamma^2 = 2\mu_{12}(M_{X_2} - M_1 - M_2)$, $\vec{q}^2_{\rm on\,shell} = 2\mu_{23}(m_{23} - M_2 - M_3)$, with $m^2_{23} = (P - p_\gamma)^2 = M^2_{X_2} - 2M_{X_2}E_\gamma$, and

$$\vec{q}^2_{\rm cm} = \frac{M_2(\vec{q} - \vec{p}_\gamma)^2 + M_3\vec{q}^2}{M_2 + M_3}. \tag{C11}$$

Note that the first exponential factor accounts for the off-shellness in the $X_2 D^{*0}\bar{D}^{*0}$ coupling, as in Eq. (39), while the second one accounts for the virtuality of the incoming mesons in the $D\bar{D}^* \to D\bar{D}^*$ and $D^*\bar{D} \to D\bar{D}^*$ T-matrices. Note that, after the inclusion of this factors, an analytical expression for the integral cannot be easily obtained, and it needs to be computed numerically.

---

[1] M. B. Voloshin and L. B. Okun, JETP Lett. **23** (1976) 333 [Pisma Zh. Eksp. Teor. Fiz. **23** (1976) 369].

[2] A. De Rujula, H. Georgi and S. L. Glashow, Phys. Rev. Lett. **38** (1977) 317.

[3] S. K. Choi *et al.* [Belle Collaboration], Phys. Rev. Lett. **91** (2003) 262001.

[4] R. Aaij *et al.* [LHCb Collaboration], Phys. Rev. Lett. **110** (2013) 222001.

[5] K. A. Olive *et al.* [Particle Data Group Collaboration], Chin. Phys. C **38** (2014) 090001.

[6] N. Brambilla, S. Eidelman, B. K. Heltsley, R. Vogt, G. T. Bodwin, E. Eichten, A. D. Frawley and A. B. Meyer *et al.*, Eur. Phys. J. C **71** (2011) 1534.

[7] J. Nieves and M. Pavon Valderrama, Phys. Rev. D **86** (2012) 056004.

[8] C. Hidalgo-Duque, J. Nieves and M. Pavon Valderrama, Phys. Rev. D **87** (2013) 076006.

[9] N. A. Törnqvist, Z. Phys. C **61** (1994) 525.

[10] C. Hidalgo-Duque, J. Nieves, A. Ozpineci and V. Zamiralov, Phys. Lett. B **727** (2013) 432.

[11] R. Molina and E. Oset, Phys. Rev. D **80** (2009) 114013.

[12] W. H. Liang, R. Molina and E. Oset, Eur. Phys. J. A **44** (2010) 479 [arXiv:0912.4359 [hep-ph]].

[13] E. S. Swanson, J. Phys. Conf. Ser. **9** (2005) 79.

[14] Z. F. Sun, Z. G. Luo, J. He, X. Liu and S. L. Zhu, Chin. Phys. C **36** (2012) 194.

[15] F.-K. Guo, C. Hidalgo-Duque, J. Nieves and M. Pavon Valderrama, Phys. Rev. D **88** (2013) 054007.

[16] F. K. Guo, C. Hanhart, Q. Wang and Q. Zhao, arXiv:1411.5584 [hep-ph].

[17] S. Godfrey and N. Isgur, Phys. Rev. D **32** (1985) 189.

[18] B. Q. Li, C. Meng and K. T. Chao, Phys. Rev. D **80** (2009) 014012.

[19] L. Maiani, F. Piccinini, A. D. Polosa and V. Riquer, Phys. Rev. D **71** (2005) 014028.

[20] S. Uehara *et al.* [Belle Collaboration], Phys. Rev. Lett. **96** (2006) 082003.

[21] B. Aubert *et al.* [BaBar Collaboration], Phys. Rev. D **81**, 092003 (2010) [arXiv:1002.0281 [hep-ex]].

[22] F.-K. Guo, C. Hanhart and U.-G. Meißner, Phys. Rev. Lett. **102** (2009) 242004.

[23] L. Liu *et al.* [Hadron Spectrum Collaboration], JHEP **1207** (2012) 126.

[24] S. Prelovsek and L. Leskovec, Phys. Rev. Lett. **111** (2013) 192001.

[25] S. Prelovsek and L. Leskovec, Phys. Lett. B **727** (2013) 172.

[26] S. Prelovsek, C. B. Lang, L. Leskovec and D. Mohler, Phys. Rev. D **91** (2015) 014504.

[27] M. Padmanath, C. B. Lang and S. Prelovsek, arXiv:1503.03257 [hep-lat].

[28] V. Baru, E. Epelbaum, A. A. Filin, C. Hanhart, U.-G. Meißner and A. V. Nefediev, Phys. Lett. B **726** (2013) 537.

[29] M. Jansen, H.-W. Hammer and Y. Jia, Phys. Rev. D **89** (2014) 014033.

[30] M. Albaladejo, C. Hidalgo-Duque, J. Nieves and E. Oset, Phys. Rev. D **88** (2013) 014510

[31] F.-K. Guo, U.-G. Meißner, W. Wang and Z. Yang, Eur. Phys. J. C **74** (2014) 3063.

[32] F.-K. Guo, U.-G. Meißner and Z. Yang, Phys. Lett. B **740** (2015) 42.

[33] F.-K. Guo, C. Hidalgo-Duque, J. Nieves, A. Ozpineci and M. Pavon Valderrama, Eur. Phys. J. C **74** (2014) 2885.

[34] F.-K. Guo, C. Hidalgo-Duque, J. Nieves, A. Ozpineci and M. Pavon Valderrama, arXiv:1411.7828 [hep-ph].

[35] F.-K. Guo, C. Hidalgo-Duque, J. Nieves and M. Pavon Valderrama, Phys. Rev. D **88** (2013) 054014.

[36] M. Pavon Valderrama, Phys. Rev. D **85** (2012) 114037.

[37] D. Gamermann, J. Nieves, E. Oset and E. Ruiz Arriola, Phys. Rev. D **81** (2010) 014029.

[38] E. Epelbaum, H. W. Hammer and U. G. Meißner, Rev. Mod. Phys. **81**, 1773 (2009).

[39] C. Hanhart, Y. S. Kalashnikova, A. E. Kudryavtsev and A. V. Nefediev, Phys. Rev. D **85** (2012) 011501

[40] B. Grinstein, E. E. Jenkins, A. V. Manohar, M. J. Savage and M. B. Wise, Nucl. Phys. B **380** (1992) 369.

[41] M. B. Wise, Phys. Rev. D **45**, 2188 (1992).

[42] G. Burdman and J. F. Donoghue, Phys. Lett. B **280**, 287 (1992).

[43] T. M. Yan, H. Y. Cheng, C. Y. Cheung, G. L. Lin, Y. C. Lin and H. L. Yu, Phys. Rev. D **46**, 1148 (1992) [Erratum-ibid. D **55**, 5851 (1997)].

[44] J. P. Lees *et al.* [BaBar Collaboration], Phys. Rev. Lett. **111**, 111801 (2013).

[45] A. Anastassov *et al.* [CLEO Collaboration], Phys. Rev. D **65**, 032003 (2002).

[46] R. Machleidt, K. Holinde and C. Elster, Phys. Rept. **149** (1987) 1.

[47] J. M. Flynn, P. Fritzsch, T. Kawanai, C. Lehner, C. T. Sachrajda, B. Samways, R. S. Van de Water and O. Witzel, PoS LATTICE **2013**, 408 (2014).

[48] F. Bernardoni *et al.* [ALPHA Collaboration], Phys. Lett. B **740**, 278 (2015).

[49] F. S. Navarra, M. Nielsen and M. E. Bracco, Phys. Rev. D **65**, 037502 (2002).

[50] F. Carvalho, F. O. Duraes, F. S. Navarra and M. Nielsen, Phys. Rev. C **72**, 024902 (2005).

[51] Y. s. Oh, T. Song and S. H. Lee, Phys. Rev. C **63**, 034901 (2001).

[52] Z. H. Li, T. Huang, J. Z. Sun and Z. H. Dai, Phys. Rev. D **65**, 076005 (2002).

[53] M. E. Bracco, M. Chiapparini, F. S. Navarra and M. Nielsen, Phys. Lett. B **659**, 559 (2008)

[54] Z. G. Wang, Eur. Phys. J. C **52**, 553 (2007).

[55] B. Osorio Rodrigues, M. E. Bracco, M. Nielsen and F. S. Navarra, Nucl. Phys. A **852**, 127 (2011).

[56] M. E. Bracco, M. Chiapparini, F. S. Navarra and M. Nielsen, Prog. Part. Nucl. Phys. **67**, 1019 (2012)

[57] J. F. Amundson, C. G. Boyd, E. E. Jenkins, M. E. Luke, A. V. Manohar, J. L. Rosner, M. J. Savage and M. B. Wise, Phys. Lett. B **296** (1992) 415.

[58] J. Hu and T. Mehen, Phys. Rev. D **73** (2006) 054003.

[59] A. Bondar *et al.* [Belle Collaboration], Phys. Rev. Lett. **108** (2012) 122001.

[60] I. Adachi *et al.* [Belle Collaboration], arXiv:1207.4345 [hep-ex].

[61] A. E. Bondar, A. Garmash, A. I. Milstein, R. Mizuk and M. B. Voloshin, Phys. Rev. D **84** (2011) 054010.

[62] M. Cleven, F.-K. Guo, C. Hanhart and U.-G. Meißner, Eur. Phys. J. A **47** (2011) 120.

[63] M. Ablikim *et al.* [BESIII Collaboration], Phys. Rev. Lett. **110** (2013) 252001.

[64] Z. Q. Liu *et al.* [Belle Collaboration], Phys. Rev. Lett. **110** (2013) 252002.

[65] T. Xiao, S. Dobbs, A. Tomaradze and K. K. Seth, Phys. Lett. B **727** (2013) 366.

[66] M. Ablikim *et al.* [BESIII Collaboration], Phys. Rev. Lett. **112** (2014) 132001.

[67] M. Ablikim *et al.* [BESIII Collaboration], Phys. Rev. Lett. **111** (2013) 242001.

[68] M. T. AlFiky, F. Gabbiani and A. A. Petrov, Phys. Lett. B **640** (2006) 238.

[69] A. V. Manohar and M. B. Wise, Camb. Monogr. Part. Phys. Nucl. Phys. Cosmol. **10**, 1 (2000).

[70] F.-K. Guo, C. Hanhart and U.-G. Meißner, Phys. Rev. Lett. **103**, 082003 (2009) [Erratum-ibid. **104**, 109901 (2010)].

[71] F.-K. Guo, C. Hanhart, G. Li, U.-G. Meißner and Q. Zhao, Phys. Rev. D **83** (2011) 034013.